**Article:**
Michoud, V, Hansen, RF, Locoge, N et al. (2 more authors) (2015) Detailed characterizations of the new Mines Douai comparative reactivity method instrument via laboratory experiments and modeling. Atmospheric Measurement Techniques, 8 (8). pp. 3537-3553. ISSN 1867-1381

https://doi.org/10.5194/amt-8-3537-2015

# Detailed characterizations of the new Mines Douai Comparative Reactivity Method instrument via laboratory experiments and modeling

V. Michoud[1], R. F. Hansen[1,2,3,*], N. Locoge[1], P. S. Stevens[2,3], S. Dusanter[1,2].

[1] Mines Douai, SAGE, F-59508, Douai, France

[2] School of Public and Environmental Affairs, Indiana University, Bloomington, IN, USA

[3] Department of chemistry, Indiana University, Bloomington, IN, USA

Correspondence to: Sebastien Dusanter (sebastien.dusanter@mines-douai .fr) and Vincent Michoud (Vincent.michoud@mines-douai.fr)

*now at : school of chemistry, University of Leeds, Leeds, UK

## Abstract

The Hydroxyl (OH) radical is an important oxidant in the troposphere, which controls the lifetime of most air quality- and climate-related trace gases. However, there are still uncertainties concerning its atmospheric budget and integrated measurements of OH sinks have been valuable to improve this aspect. Among the analytical tools used for measuring total OH reactivity in ambient air, the Comparative Reactivity Method (CRM) is spreading rapidly in the atmospheric community. However, measurement artifacts have been highlighted for this technique and additional work is needed to fully characterize them.

In this study, we present the new Mines-Douai CRM instrument, with an emphasis on the corrections that need to be applied to ambient measurements of total OH reactivity. Measurement artifacts identified in the literature have been investigated, including: (1) a correction for a change in relative humidity between the measurement steps leading to different OH levels, (2) the formation of spurious OH in the sampling reactor when hydroperoxy radicals ($HO_2$) react with nitrogen monoxide (NO), (3) not operating the CRM under pseudo-first-order kinetics, and (4) the dilution of ambient air inside the reactor. The dependences of these artefacts to various measurable parameters, such as the pyrrole-to-OH ratio and the bimolecular reaction rate constants of ambient trace gases with OH, have also been studied. Based on these observations, parameterizations are proposed to correct ambient OH reactivity measurements. On average, corrections of 5.2±3.2 $s^{-1}$, 9.2±15.7 $s^{-1}$, and 8.5±5.8 $s^{-1}$ were respectively observed for (1), (2) and (3) during a field campaign performed in Dunkirk, France (summer 2014).

Numerical simulations have been performed using a box model to check whether experimental observations mentioned above are consistent with our understanding of the chemistry occurring in the CRM reactor. Two different chemical mechanisms have been shown to reproduce the magnitude of corrections (2) and (3). In addition, these simulations reproduce their dependences on the Pyrrole-to-OH ratio and on bimolecular reaction rate constants of gases reacting with OH. The good agreement found between laboratory experiments and model simulations gives confidence in the proposed parameterizations. However, it is worth noting that the numerical values given in this study are suitable for the Mines Douai instrument and may not be appropriate for other CRM instruments. It is recommended that each group characterizes its own instrument following the recommendations given in this study.

An assessment of performances for the Mines Douai instrument, including a propagation of errors from the different corrections, indicates a limit of detection of 3.0 $s^{-1}$ and total uncertainties of 17-25% for OH reactivity values higher than 15 $s^{-1}$ and $NO_x$ mixing ratios lower than 30 ppbv.

## 1 Introduction

The hydroxyl (OH) radical is known to be the main daytime oxidant in the troposphere (Levy, 1972), leading to the oxidation of most atmospheric trace gases, including climate related compounds such as methane, and the formation of harmful secondary pollutants such as ozone ($O_3$) and Secondary Organic Aerosols (SOA). Due to the key role of OH in atmospheric chemistry, it is important to correctly describe the OH budget in atmospheric models. Field campaigns including OH measurements have been carried out to assess our understanding of photochemical processes controlling the OH budget (see Stone et al., 2012, as a review). In these studies, measurements of OH concentrations are often compared to predictions from photochemical models that are constrained by measured concentrations of long-lived species and environmental parameters (e.g. Carslaw et al., 2002; Martinez et al., 2003; Dusanter et al., 2009; Hofzumahaus et al., 2009; Michoud et al., 2012). This approach allows testing our understanding of different aspects of the OH chemistry, i.e. sources, sinks and propagation reactions.

Volatile Organic Compounds (VOCs) are of particular interest for the OH chemistry due to the presence of a large number of reactive species ($10^4$-$10^5$), emitted by natural and anthropogenic sources, or formed photochemically (Goldstein and Galbally, 2007). However,

measurements of VOCs are challenging and measuring an exhaustive suite of VOCs is unfeasible using current analytical techniques. During field campaigns, only 60-70 VOCs are usually monitored, which is orders of magnitudes lower than expected in the atmosphere (Goldstein and Galbally, 2007). Therefore, there are legitimate concerns regarding the completeness of the measured pool of VOCs and the use of these measurements to characterize the total sink of OH.

To address this issue, an integrated measurement of the total sink of OH, referred as total OH reactivity, has been proposed by Calpani et al. (1999) and Kovacs and Brune (2001). OH reactivity measurements are important for several reasons: (i) it allows to better constrain photochemical models during radical closure exercises and to test the representativeness of the chemical mechanism used in these models; (ii) since OH exhibits steady state concentrations in the atmosphere due to its short lifetime, the measured total OH reactivity can be used together with measured OH concentrations to calculate total production rates of OH. Comparing the latter to production rates calculated from measured OH precursors provides a critical test of our understanding of OH sources (Whalley et al., 2011); (iii) the total OH reactivity calculated from measured trace gases can be compared to the measurements to see whether unidentified reactive species are present in ambient air, with the goal of assessing their importance for atmospheric chemistry. If statistically significant, the difference observed between measurements and calculations is referred as "missing OH reactivity".

Large missing OH reactivity is often found in different types of environments (e.g. Di Carlo et al., 2004; Lou et al., 2010; Dolgorouky et al., 2012; Edwards et al., 2013; Hansen et al., 2014) highlighting the presence of important unmeasured reactive compounds. This missing reactivity has been attributed to unidentified primary biogenic VOCs or unmeasured oxidation products of primary VOCs that has yet to be identified.

The first techniques proposed to measure total OH reactivity, the Total OH Loss rate Method (TOHLM) (Kovacs and Brune, 2001) and the Pump-Probe method (Sadanaga et al., 2004), require monitoring OH radicals using laser apparatus, making them costly, and require highly skilled operators. More recently, a novel technique called Comparative Reactivity Method (CRM) has been proposed in the literature (Sinha et al., 2008). This technique does not require direct OH measurements and is based on monitoring competitive reactions of OH with a reference molecule (pyrrole) and ambient trace gases inside a sampling reactor. The total OH reactivity is derived from a series of measurement steps during which the pyrrole concentration is quantified using a specific detector, being most of the time a Proton Transfer

Reaction-Mass Spectrometer (PTR-MS). An interesting advantage of CRM instruments is the small sampling flow rate (a few hundreds of SCCM) that is needed compared to TOHLM and Pump-Probe instruments (a few SLPM). This advantage allows extending its use to small atmospheric chambers (Nölscher et al., 2012b) and cuvettes (Nölscher et al., 2013) experiments.

CRM instruments have been widely used during field campaigns (Sinha et al., 2008; Sinha et al., 2010; Kim et al., 2011; Dolgorouky et al., 2012; Nölscher et al., 2012a; Sinha et al., 2012; Nölscher et al., 2013; Hansen et al., 2015; Zannoni et al., 2015) and chamber experiments (Nölscher et al., 2012b; Nölscher et al., 2014) since its development and new research groups are developing similar systems. Its deployment in the field led to important observations related to high missing reactivity. For instance, high levels of missing reactivity were observed during heat stressed conditions in a boreal forest (Nölscher et al., 2012a) due to unmeasured reactive VOCs from primary or secondary origins; as well as during the transport of aged continental air masses in an urban environment in Paris (Dolgorouky et al., 2012), likely due to unmeasured (multi-)oxidized compounds formed from the oxidation of anthropogenic emissions.

A new CRM instrument has been developed and coupled to a Proton Transfer Reaction-Time of Flight Mass Spectrometer (PTR-ToFMS) at Mines Douai (France). This instrument has been compared to the pump-probe technique in an urban environment (Hansen et al., 2015) and to another CRM instrument at a remote site (Zannoni et al., 2015). Generally, good agreements have been observed and reasons for some deviations have been identified.

However, this technique requires multiple corrections (Hansen et al., 2015), especially to account for an artifact generated by ambient NO (Sinha et al., 2008; Dolgorouky et al., 2012), which limited its use to low $NO_x$ environments, except for two previous studies (Dolgorouky et al., 2012; Hansen et al., 2015). Other corrections are also needed to derive reliable measurements of total OH reactivity due to (i) changes in humidity between the different measurement steps, (ii) not operating the CRM under pseudo-first-order kinetics (Sinha et al., 2008), (iii) the dilution of ambient air inside the reactor. While the need for correcting the measurements is known from the early use of CRM, a comprehensive characterization of these corrections as yet to be published.

In this study, we describe the CRM instrument constructed in Mines Douai (MD-CRM), highlighting the modifications made on the setup since its first deployment (Hansen et al., 2015). A detailed description of the corrections needed to derive accurate OH reactivity measurements is presented based on intensive laboratory experiments. Furthermore,

simulations performed using different chemical mechanisms are compared to experimental observations to investigate our understanding of the chemistry occurring inside the sampling reactor. Finally, figures of merit such as limit of detection and measurement uncertainties are assessed.

## 2 The Comparative Reactivity Method (CRM)

### 2.1 General Principle

As mentioned above, the Comparative Reactivity Method relies on monitoring how a reference molecule competes with ambient trace gases to react with artificially produced OH radicals inside a sampling reactor. This technique has been first described by Sinha et al. (2008) and has been discussed in detail by Hansen et al. (2015). Briefly, a reference molecule that is not present in the atmosphere (pyrrole, $C_4H_4NH$), dry nitrogen ($N_2$), and dry zero air are first introduced into a reactor equipped with a UV mercury lamp. During this step, while the lamp is ON, OH is not produced inside the reactor due to the dry conditions. The pyrrole concentration (C1) is monitored using a suitable detector, most of the time by PTR-MS at the protonated m/z 68. C1 corresponds to the initial concentration of pyrrole inside the reactor after potential photolysis due to photons leaking inside the reactor. Then, dry gases (zero air and $N_2$) are replaced by wet gases to generate OH radicals from $H_2O$ photolysis. A decrease of the pyrrole concentration (C2) is observed due to its reaction with OH. Once the C2 concentration is acquired, wet zero air is replaced by ambient air and competitive OH reactions occur between pyrrole and ambient trace gases. This competition leads to an increase of the pyrrole concentration to C3. A schematic of the pyrrole levels observed during these three measurement steps is shown in Figure 1 (insert). The OH reactivity is calculated using Eq. ( 1), assuming first order kinetics, with $k_p$ corresponding to the bimolecular rate constant of the reaction between pyrrole and OH ($1.2\ 10^{-10}$ $cm^3$ $molecules^{-1}$ $s^{-1}$ at 25°C (Atkinson et al., 1984; Dillon et al., 2012)).

$$k_{OH} = \frac{(C3 - C2)}{(C1 - C3)} \cdot k_p . C1 \qquad (1)$$

The conventional method described above to record C1 takes a long time, i.e. 2-3 hours, since completely dry conditions are needed inside the reactor. In addition, this method likely leads to an overestimation of pyrrole photolysis inside the reactor due to residual water. For

these reasons, the scavenger method described in Zannoni et al. (2015) was preferred for this study. As described in Zannoni et al. (2015), this method consists in introducing an elevated concentration of a specific species (here propane at approximately 900 ppm) acting as an OH scavenger. This approach is advantageous since it takes only a few minutes to record a stable C1 concentration and it can be performed keeping the wet conditions that are needed for other measurement steps.

As stated in the introduction, this technique suffers from several measurement artifacts for which the measured OH reactivity values need to be corrected. Corrections, in the order of their application in the data processing, are:

- Correction on C2 for RH variations between C2 and C3;
- Correction on C3 for the spurious production of OH from the reaction between $HO_2$ (mainly formed from $H_2O$ photolysis) and ambient NO;
- Correction on OH reactivity values calculated from Eq. ( 1 ) for not operating the instrument under pseudo-first-order conditions;
- Correction on OH reactivity values for dilution, due to the addition of $N_2$ inside the reactor.

## 2.2 Description of the Mines Douai CRM instrument

A description of the CRM instrument developed at Mines Douai (MD-CRM) as well as its operating conditions are given in this section. The MD-CRM instrument has been previously described in Hansen et al. (2015) and a schematic is shown in Figure 1. Several improvements have been performed since its first deployment during the intercomparison exercise presented in Hansen et al. (2015), in particular to lower pyrrole photolysis below 5% by changing the UV mercury lamp position in the setup (Laser Components, model 11SC-1). As a consequence, the photolysis of other trace gases in the reactor has also been reduced. As discussed in Hansen et al. (2015), photolysis of VOCs inside the reactor led to unaccounted OH reactivity during tests performed using synthetic VOC mixtures. Up to 55% of the OH reactivity was not measured for a complex OVOC mixture. For the current MD-CRM setup, direct observations of VOC photolysis inside the reactor indicate less than 1% of photolysis for OVOCs such as methanol, acetaldehyde, acetone, etc… (see Table S1). In contrast to what was observed with the prior version of this instrument, the new setup allows reconciling

measured and calculated reactivity within 9% for similar VOC mixtures (see supplementary material S1).

Pyrrole (Praxair, 10 ppm in $N_2$) and $N_2$ (Air Liquide, alpha gaz 2; or Praxair, $N_2$ 6.0) were introduced into a glass flow reactor built by the Max Planck Institut für Chemie (Mainz, Germany) at flow rates of 2.3 and 70 mL $min^{-1}$, respectively. $N_2$ was humidified by passing it through a water bubbler or was kept dry, depending on the measurement step. The C1-C2-C3 pyrrole mixing ratios were monitored by a PTR-ToFMS instrument (Kore Technology, second generation), whose sampling flow rate was regulated at 145 mL $min^{-1}$ using a mass flow controller (MFC) (MKS inst, 200 sccm). Dry zero air was produced by an air generator (CLAIND, model 2301TOC). For wet conditions, humid zero air was generated by sampling ambient air through a catalytic converter made of a stainless steel tubing filled with Pt wool held at 350°C (prior 2014). This setup generates zero air at the same relative humidity (RH) as ambient air. More recently (after 2014), humid zero air was generated using a similar air generator as for the dry conditions. The flow was split and passed through two MFCs (MKS inst., 500sccm), one of them being sent through a water bubbler. The two flows were then mixed back together to generate wet zero air at a specific RH. Two RH probes (Measurements Specialties Inc, model HM1500LF) were mounted in this set up for measuring RH in both the generated humidified air and the ambient air. The flow rates of the two MFCs were controlled using a LabView (National instrument) program to get the same RH in zero and ambient air. This new setup was designed for high $NO_x$ environments since these species are not suppressed from ambient air using a catalytic converter, which in turn can lead to erroneous measurements of C2. Finally, a pump draws 240 mL $min^{-1}$ at the end of the reactor. For this configuration, approximately 310 mL $min^{-1}$ of zero air (during C1 and C2) or of ambient air (during C3) are sampled by the CRM instrument.

To minimize the residence time inside the sampling line, a Teflon pump is added upstream of the reactor to sample ambient air at approximately 1 L $min^{-1}$, with the excess going to an exhaust. This pump is only installed during field campaigns and all the laboratory tests presented in this study were conducted without it.

## 2.3 Description of the laboratory experiments

For laboratory tests presented in this study, the CRM was usually kept under C2 conditions (humid zero air provided to the reactor) and gas standards of different natures (VOCs or $NO_x$) were directly injected in the line bringing zero air to the reactor as shown in

Figure 1. During these experiments, the C1 level was approximately 57 ppb, corresponding to a photolysis of 5% of 60.4 ppb of pyrrole introduced inside the reactor, and the C2 level ranged from 17-43 ppb, depending on the level of RH used during each experiment.

### 2.3.1 Changes in RH between C2 and C3

While the use of a catalytic converter or a dynamic humidification of zero air helped to reduce differences in RH between C2 and C3, small differences were still observed. Since the concentration of OH inside the reactor is driven by water photolysis, a small difference in RH can lead to significant different OH levels between C2 and C3, and as a consequence to an artifact in the C2 measurement (Sinha et al., 2008). Therefore, a correction is directly applied to the pyrrole concentrations measured during C2 as proposed in Dolgorouky et al. (2012). To assess this correction, experimental determinations of the C2 sensitivity to humidity were performed measuring C2 at various RH before, during, and after field campaigns. These tests were made by introducing various flow rates of dry zero air (from 50 to 300 sccm) inside the sampling line. The dilution of humid ambient air with dry zero air allowed to change RH over a large range of relative humidity (typically 20-60%, Figure 2).

To track relative humidity during these experiments and during ambient measurements of OH reactivity, we use the ratio between m/z 37 (cluster ion $H_3O^+.H_2O$) and m/z 19 ($H_3O^+$) monitored by PTR-ToFMS. Indeed, $H_3O^+$ ions can cluster in the drift tube of PTR-MS instruments (DeGouw and Warneke, 2007) to form water clusters ($H_3O^+(H_2O)_n$) whose levels depend on relative humidity inside the PTR-MS reactor. A linear relationship was found between RH and the m/z 37-to-m/z 19 ratio (referred as m37/m19 ratio in the following) during laboratory tests (not shown).

### 2.3.2 NO and $NO_2$ artifacts

As mentioned above, OH radicals are artificially generated in the sampling reactor from water photolysis using a mercury lamp. A drawback of this method is the formation of a similar amount of $HO_2$ radicals since hydrogen atoms are formed in the water photolysis process, which then quickly react with oxygen to form $HO_2$. When ambient NO is sampled inside the reactor, these $HO_2$ radicals can be rapidly converted into OH radicals. This secondary formation of OH leads to differences in OH levels between C2 and C3, and therefore to an artifact in the C3 measurement. To assess the required correction for C3

values, different amounts of NO (from 6 to 120 ppb) were introduced inside the reactor while sampling humid zero air. Similar experiments were conducted by adding ethane and isoprene together with NO in the sampling reactor, leading to VOC-induced reactivity values of 22.2 $s^{-1}$ and 36.6 $s^{-1}$, respectively. These experiments have been conducted at different apparent pyrrole-to-OH ratios ranging from 1.6 to 3.9 and determined by equation ( 2). This ratio is used to gauge the kinetic regime in the CRM reactor (Sinha et al., 2008). For simplicity, this apparent pyrrole-to-OH ratio (supplementary material S3) is referred as the pyrrole-to-OH ratio in the following. In practice, this ratio is adjusted by changing RH in the reactor, which in turn leads to a change in OH levels.

$$\frac{Pyrrole}{OH} = \frac{C1}{C1 - C2} \quad (2)$$

While $NO_2$ is not expected to lead to the formation of secondary OH inside the reactor, its conversion into NO through photolysis or other chemical processes can cause an artifact. To test the effect of $NO_2$ on C3 measurements, we followed the same procedure than described above for NO. Different amounts of $NO_2$ (from 60 to 410 ppb) were introduced inside the CRM reactor when sampling humid zero air at pyrrole-to-OH ratios ranging from 1.6-3.2.

### 2.3.3 Artifact due to not operating the CRM under pseudo-first-order conditions

Measured OH reactivity values are calculated using Eq. ( 1 ). In this equation, pseudo-first-order conditions are assumed for pyrrole, i.e. pyrrole concentrations are at least several times higher than OH concentrations. However, operating conditions used for CRM instruments do not comply with this assumption and the calculated values (Eq. 1) need to be corrected. To assess this correction, several gas standards (ethane, ethene, propane, propene, and isoprene) were introduced inside the CRM reactor at different concentrations. It allows comparing the calculated OH reactivity generated by the standards (reactivity ranging from 6.5 to 65 $s^{-1}$) to the OH reactivity measured using equation (1). These experiments have been conducted at pyrrole-to-OH ratios ranging from 1.4-2.6.

## 3 Model Descriptions

The laboratory experiments performed in this study were compared to results from zero-dimensional (0D) model simulations to test our understanding of the chemical processes occurring inside the reactor. These simulations were conducted using two different mechanisms: a simple mechanism and the Master Chemical Mechanism v3.2 ((http://mcm.leeds.ac.uk/MCM) (Jenkin et al., 1997; Saunders et al., 2003; Jenkin et al., 2003; Bloss et al., 2005; Jenkin et al., 2012). The two chemical mechanisms are presented in the following. The FACSIMILE solver was used to solve the differential equations generated from the different mechanisms. These simulations have been conducted constraining the box model by initial concentrations of Pyrrole, OH, and different gas standards used during the laboratory experiments. Both models were used to simulate the pyrrole modulations (C1-C2-C3).

Simulations were performed considering an ideal case where a finite amount of OH is introduced in a fresh mixture of air/standard trace gases, assuming plug-flow conditions in the reactor. In this scenario, (i) a small amount of OH is introduced in the air mixture, (ii) OH fully reacts with trace gases leading to oxidation products, (iii) the air mixture is refreshed at the OH injector tip before more OH is added. However, OH is produced continuously at the injector tip and OH can potentially react with byproducts and peroxy radicals previously formed since constant flows are maintained. While the simulation procedure used in this study may need some refinements, it is however interesting to compare trends observed during experimental tests to model simulations when some parameters such as the pyrrole-to-OH ratio are varied.

### 3.1 Simple Mechanism

The simple mechanism (Table S2, supplementary material) is an improved version of the mechanism used by Sinha et al. (2008) since it includes additional inorganic chemistry reactions from IUPAC 2001. The addition of these inorganic reactions aims at taking into account cross- and self-reactions of radical species (mainly $OH+HO_2$ and $HO_2+HO_2$), as well as termination ($OH + NO_2$, $OH + NO$), and propagation ($HO_2 + NO$) reactions of $NO_x$ with radicals. The latter is the reaction leading to the spurious formation of OH during C3 measurements.

Apart from these inorganic reactions, reactions of OH with pyrrole ($1.2\ 10^{-10}$ $cm^3$ $molecules^{-1}$ $s^{-1}$; Atkinson et al., 19984; Dillon et al., 2012) and with a surrogate hydrocarbon ($5.0\ 10^{-12}$ $cm^3$ $molecules^{-1}$ $s^{-1}$, typical of C5-C6 alkanes or aromatics) are included in the

mechanism, both leading to a similar surrogate of organic peroxy radicals. In addition, reactions describing the chemistry of this surrogate $RO_2$ are included: $RO_2+RO_2$, $RO_2+HO_2$, $RO_2+NO = RO+NO_2$, and $RO+O_2 = HO_2$; reaction rate constants for these reactions are those for methylperoxy radical ($CH_3O_2$) ($3.4\ 10^{-13}$, $5.2\ 10^{-12}$; $7.7\ 10^{-12}$ and $1.9\ 10^{-15}$ $cm^3$ $molecules^{-1}$ $s^{-1}$, respectively). This mechanism leads to a total number of 42 reactions.

### 3.2 Master Chemical Mechanism (MCM)

A more comprehensive analysis of the chemistry occurring inside the CRM reactor has been conducted using the MCM v3.2. The use of a detailed mechanism such as MCM aims at better representing the chemistry of peroxy radicals. Indeed, a detailed speciation of peroxy radicals that are formed during the oxidation of primary organic compounds is included in this mechanism. For this study, a MCM subset was extracted for inorganic reactions, ethane, propane, ethene, propene and isoprene. The 2(5H)-Furanone chemistry was also extracted to use it as a surrogate for the pyrrole chemistry since the latter is not included in MCM. This subset of the MCM led to a mechanism containing 502 species and 1610 reactions.

The surrogate used for pyrrole, 2(5H)-Furanone ($C_4H_4O_2$), is named BZFUONE in MCM. This surrogate was chosen to get a molecule whose molecular structure is as close as possible to the pyrrole structure. It is also a cyclic compound but with an oxygen atom inside the ring instead of a nitrogen atom. BZFUONE also contains a carbonyl group in α position of the oxygen atom, which is not the case for pyrrole. We acknowledge that this is a crude approach to account for the pyrrole chemistry in the mechanism. To the best of our knowledge, there is no information about the pyrrole chemistry in the literature and a more rigorous approach was not possible. There is, therefore, a need for laboratory studies to investigate the photodegradation of pyrrole in atmospheric chambers.

The MCM was modified as the following. The reaction of pyrrole with OH included in the mechanism leads to the formation of the same $RO_2$ than the reaction of BZFUONE with OH. However, the reaction rate constant was set at the same value than in the simple mechanism (i.e. $1.2\ 10^{-10}$ $cm^3$ $molecules^{-1}$ $s^{-1}$). The same approach was used for the reaction of pyrrole with $O_3$, using a rate constant of $1.57\ 10^{-17}$ $cm^3$ $molecules^{-1}$ $s^{-1}$ (Atkinson et al., 1984).

All the simulations were conducted using operating conditions used during laboratory investigations, i.e. T=20°C and P=760torr, except for the relative humidity (RH). Indeed, simulations were performed for completely dry conditions (RH=0%) and for saturated conditions (RH=100%).

## 4 Dunkirk field campaign

Preliminary results of OH reactivity measurements performed during a campaign are presented in sections 5.4 as an example to discuss how the raw data is processed and how uncertainties are estimated.

This campaign took place at a ground site located inside the harbour area of Dunkirk (51.0523°N; 2.3540°E), France, from 26 June to 31 July 2014. This site was influenced by industrial, urban, and marine emissions (Moderate to high $NO_x$: <1 ppb to 150 ppb). Sequential measurements of OH reactivity and VOCs were performed with the MD-CRM instrument with time resolutions of 20 min for OH reactivity and 10 min for VOCs. This approach was especially designed for an identification of potential reactive species that are responsible for missing OH reactivity. Two different high flow rate sampling inlets (approximately 1 SLPM) were used for measuring OH reactivity and VOCs. These inlets were 5-m long and were made of ¼ inch Teflon tubing. The VOC sampling line was heated at 50°C while the sampling line for the CRM was kept at ambient temperature.

Collocated measurements of 40 VOCs, inorganic species ($NO_x$, $O_3$, $SO_2$, CO, $CO_2$), meteorological parameters and aerosols were also performed. The results from this campaign will be presented in a forthcoming publication.

## 5 Results and Discussions

Experimental parameterizations of the different corrections applied to the MD-CRM measurements are presented in this section, as well as the comparison to simulations conducted with the box models described above. We then present how the raw data from the Dunkirk field campaign was processed and a detailed assessment of the detection limit and measurement uncertainties.

### 5.1 Correction for changes in RH between C2 and C3

Figure 2 shows the results of three experiments conducted to assess the sensitivity of C2 to humidity during the Dunkirk field campaign. The decrease of C2 with relative humidity is linear and can therefore be easily corrected during ambient measurements. A corrected C2 value is calculated for the RH value observed during the C3 measurement, taking into account

its dependence to humidity (see Figure 2) and the difference in the m37/m19 ratio monitored during C2 and C3 (see Eq. ( 3 )). In this equation, p corresponds to the slope of the linear regression between C2 and the m37/m19 ratio. The uncertainty on the slope was estimated, to be 12% (1σ) from laboratory and field experiments. The corrected C2 value is then used in Eq. ( 1 ) to calculate the OH reactivity.

$$C2_{corrected} = C2 + p\left[\left(\frac{m37}{m19}\right)_{C3} - \left(\frac{m37}{m19}\right)_{C2}\right] \quad (3)$$

The three experiments displayed in Figure 2 highlight the reproducibility of this determination over a period of ambient measurements longer than a month. The black and red segments are the mean and maximum variations of m37/m19 observed between C2 and C3 during the field campaign, respectively. These segments indicate the amplitude of the correction that had to be applied to measured C2 values (0.1 and 3.9 ppbv for the mean and the maximum variations, respectively). The average correction was 5.2±3.2 $s^{-1}$ (1σ) for the whole field campaign.

## 5.2 Corrections for NO and $NO_2$ artifacts

### 5.2.1 NO artifact - dependence on the Pyrrole-to-OH ratio

Figure 3 shows experiments conducted to quantify the C3 dependence on NO due to the spurious formation of OH from $HO_2$+NO. These experiments were made at different Pyrrole-to-OH ratios by sampling humid zero air. A total of 4 laboratory experiments (3 shown in Figure 3) were conducted at Pyrrole-to-OH ratios ranging from 1.6-3.9, covering the typical range of ratios observed during ambient measurements (generally from 1.6 to 2.2).

The variation of C3 (ΔC3) is computed as the difference between an expected C3 and the measured C3, since a decrease in the pyrrole mixing ratio is observed when NO increases. The expected C3 is calculated using measured levels of C1 and C2, and an expected OH reactivity due to NO (from 1.1 to 30.9 $s^{-1}$). Knowing these three terms, one can calculate the expected C3 from equation ( 1 ). To indicate the level of correction brought to the OH reactivity measurements, the absolute change in total OH reactivity for the experiment conducted at a pyrrole-to-OH ratio of 2.2 is also given in Figure 3 (right axis).

As expected, a decrease of the pyrrole mixing ratio is observed when NO is introduced inside the reactor at a constant pyrrole-to-OH ratio. However, the variation of C3 with NO is

not linear and varies with the Pyrrole-to-OH ratio. Indeed, the difference between the expected and measured C3 indicates a plateau at high NO mixing ratios. In addition, the amplitude of this NO artifact increases with the Pyrrole-to-OH ratio, i.e. with decreasing OH concentrations in the reactor, C1 being kept constant for all experiments.

A quadratic regression forced through the origin was applied to fit the observations (solid lines in Figure 3). It is interesting to note that the parameters for the quadratic regression vary linearly with the Pyrrole-to-OH ratios (see middle and bottom panels in Figure 3). It is thus possible to interpolate the parameters from the quadratic regression to the Pyrrole-to-OH ratios observed during field measurements to calculate the correction to apply to C3 (Eqs. ( 4-( 7):

$$C_3^{corrected} = C_3^{measured} + \Delta C_3 \quad (4)$$

$$\text{With: } \Delta C_3 = a[NO]^2 + b[NO] \quad (5)$$

$$\text{With: } a = a_1 \frac{Pyrrole}{OH} + a_2 \text{ and } b = b_1 \frac{Pyrrole}{OH} + b_2 \quad (6)$$

$$\text{So: } \Delta C_3 = \left(a_1 \frac{Pyrrole}{OH} + a_2\right)[NO]^2 + \left(b_1 \frac{Pyrrole}{OH} + b_2\right)[NO] \quad (7)$$

The experiment performed using dry zero air (Pyrrole-to-OH ratio of 3.9) is not taken into account in the linear regressions displayed in the bottom panels of Figure 3 because a deviation from the linearity is observed. Not considering this point is acceptable since completely dry conditions are never observed during ambient measurements, for which Pyrrole-to-OH ratios are always lower than 2.6. These experiments were also carried out by adding different gas standards (ethane and isoprene) inside the reactor at the same time than NO. The gas standard additions were adjusted to get OH reactivity values from VOCs ranging from 22.2 to 36.6 $s^{-1}$. These experiments and the discussion on the effect of adding a VOC are given in the supplementary material (Fig. S2). Briefly, no clear impact was found on the NO artifact, suggesting that the correction characterized above is suitable for ambient measurements. This correction can be applied during field measurements using pyrrole-to-OH ratios that are continuously monitored by the CRM instrument and measured ambient mixing ratios of NO.

### 5.2.2 $NO_2$ artifact

Figure 4 (Top panel) displays the changes in C3 with $NO_2$ mixing ratios inside the reactor for three different Pyrrole-to-OH ratios. As for NO, the introduction of $NO_2$ in the reactor leads to a decrease of the pyrrole mixing ratio. ΔC3 also appears to be non-linear with $NO_2$, exhibiting a plateau at mixing ratios higher than approximately 150 ppb. However, no clear difference is observed for experiments conducted at various Pyrrole-to-OH ratios.

The artifact caused by $NO_2$ may be due to its conversion into NO before or within the reactor. To determine the fraction of $NO_2$ converted into NO, we calculated the amount of NO needed (based on the experiments presented in section 5.2.1) to explain the changes observed on C3 when $NO_2$ was introduced inside the reactor. Based on the entire set of $NO_2$ experiments, these calculations led to a conversion ranging from 16% to 37%, with an average value of 24% (±9%, 1σ) (Figure 4 bottom panel).

Further work was performed to study the conversion of $NO_2$ inside the MD-CRM instrument. A $NO_x$ analyzer (Thermo Environmental Instruments, model 42C) was connected to the reactor exhaust instead of the PTR-MS while $NO_2$ was introduced at the reactor inlet. Since the sampling flow rate of the $NO_x$ analyzer was 600 sccm, 460 sccm of zero air was added in the sampling line of the $NO_x$ analyzer to only sample 140 sccm from the reactor, similar to the sampling flow rate from the PTR-MS instrument. Large mixing ratios of NO were observed at the exit of the reactor (between 25 and 30% of total $NO_x$) when the mercury lamp was OFF, while low NO mixing ratios (~8.7% of total $NO_x$) were observed at the reactor inlet. This result indicates that $NO_2$ is not converted into NO by photolysis but rather by heterogeneous chemical processes, probably on stainless steel pieces upstream and downstream the glass reactor. The replacement of all the stainless steel pieces in the set-up is planned in the future to avoid, or at least to reduce, this $NO_2$ conversion.

Using a similar approach than for NO, the correction to apply on C3 for $NO_2$ can be calculated using a quadratic regression shown in Fig. 4, independently of the pyrrole-to-OH ratio and using the measurements of ambient $NO_2$. It is worthwhile noting that the amplitude of the correction is significantly lower for $NO_2$ compared to NO.

### 5.2.3 Comparison of model simulations to laboratory observations

Box model simulations were compared to experimental observations discussed above. It is worth noting that pyrrole-to-OH ratios reported for the simulations were calculated using the same approach than during laboratory experiments, i.e. using Eq. ( 2). As already mentioned, the calculations do not lead to the real pyrrole-to-OH ratios (calculated from

concentrations of pyrrole and OH used to initialize the model) but to apparent ratios since C1-C2 is not the total OH mixing ratio inside the reactor but the amount of OH reacting with pyrrole. Since the mechanisms include self- and cross-reactions of radicals, all the OH introduced in the model does not react with pyrrole, and true pyrrole-to-OH ratios are lower than the measured apparent ratios. A comparison of real and apparent ratios is given in the supplementary material (Fig. S3). For instance, an apparent ratio of 2 corresponds to a real ratio of approximately 1 for simulations conducted under dry conditions with the simple mechanism and initial mixing ratios of OH and $HO_2$ set at the same value in the model.

Initial OH mixing ratios were set in the simulations to reproduce apparent pyrrole-to-OH ratios observed during laboratory experiments. Real mixing ratios of OH inside the reactor were also determined experimentally by introducing a large amount of Isoprene (3 ppmv) in the presence or absence of OH. OH mixing ratios were calculated from the consumption of isoprene and compared to levels set in the model to reproduce laboratory observations (see supplementary material, Fig. S4). It was found that OH mixing ratios set in the model agree within uncertainties with experimental determinations, indicating that initial conditions used in the model are representative of the real OH levels inside the reactor.

Experimental results related to the NO artifact, as well as simulations performed using the two mechanisms described in section 3 (simple mechanism and MCM), are displayed in Figure 5.

Both models predict a change in C3 that is similar to laboratory observations when NO increases inside the reactor. Indeed, the models predict that ΔC3 first increases with NO and levels off after the addition of a certain amount (> 90 ppbv). This behavior indicates that all $HO_2$ radicals are titrated when a threshold of NO is reached and further addition of NO does not cause any additional formation of OH through the NO + $HO_2$ reaction. Furthermore, both models also predict that ΔC3 becomes larger at higher pyrrole-to-OH ratios, similar to experimental observations. A potential reason for this behavior is that the concentrations of both OH and $HO_2$ are lower at higher pyrrole-to-OH ratios, since the pyrrole concentration is held constant in all experiments and simulations (C1 = 55 ppb). Lower concentrations of radicals lead to a slower reaction rate between OH and $HO_2$. As a consequence, OH radicals formed from NO + $HO_2$, even in lower quantity, will preferentially react with pyrrole rather than $HO_2$, leading to a larger change in ΔC3.

Significant differences are found between the simulations conducted using the two mechanisms. Indeed, simulations performed using the simple mechanism leads to an overestimation of the NO interference by up to 27% while simulations performed using MCM

leads to an underestimation of 10% at most. These differences lie in the way the chemistry of organic peroxy radicals is treated. In the simple mechanism, each reaction of OH with an organic compound gives the same $RO_2$ radical, which propagates to $HO_2$ after reaction with NO and $O_2$ without any other byproduct. In MCM, a more complex chemistry is included since specific peroxy radicals are formed for each reacting organic molecule and closed-shell byproducts are generated from the peroxy radical reactions, which can further react with OH. Since, the simulations from the two mechanisms encompass the experimental results, one can conclude than the lack of speciation for $RO_2$ radicals and of secondary chemistry in the simple mechanism do not allow to correctly reproduce the laboratory observations, while the secondary chemistry included in the MCM, in particular the proxy used to account for the pyrrole chemistry (BZFUONE), is not fully representative of the chemistry occurring inside the CRM reactor.

It is interesting to note that both mechanisms lead to coefficients (a and b) of the quadratic regressions (ΔC3 vs. pyrrole-to-OH) similar to that observed for the laboratory experiments (see bottom panels of Figure 5).

Since all the simulations described above were conducted under dry conditions, the influence of humidity was tested by repeating the same simulations at a relative humidity of 100% (see supplementary material, Fig. S5). A decrease of ΔC3 of less than 10% was observed at all pyrrole-to-OH ratios. This trend can be due to a water enhancement of the $HO_2$ self-reaction rate, reducing the secondary formation of OH, and hence the NO artifact. In practice, the pyrrole-to-OH ratios are directly linked to relative humidity inside the reactor, since OH levels depend on the amount of water available for photolysis. Simulation results that have to be compared to experimental results are between these two extreme cases (dry and RH saturated), being closer to dry condition results at higher Pyrrole-to-OH ratios and vice versa. However, only small differences are observed between dry and RH saturated conditions and the simulations made under dry conditions are suitable for this comparison.

The effect of adding gas standards (isoprene and ethane) in the simulations has also been investigated and is displayed in Fig. S6. Simulations made using MCM suggest a small dependence of ΔC3 (~6.1±1.1%) on OH reactivity for values in the range 20-40 $s^{-1}$, especially at high NO concentrations (NO > 100 ppb). This difference is small and is within measurement uncertainties.

Simulations presented above were performed assuming no $O_3$ in the reactor. However, photolysis of $O_2$ may occur inside the reactor due to the UV lamp and may lead to a significant $O_3$ concentration. The influence of $O_3$ on simulated NO artifacts was tested using

an initial $O_3$ mixing ratio of 200 ppb with the MCM (see supplementary material, Fig. S12.2). The 200 ppb of ozone correspond to the value measured at the exhaust of the reactor under dry conditions, using an ozone analyzer (Environnement-SA, model O3-42M). Adding ozone in the simulations only leads to a small decrease of approximately 3% for the NO artifact, independent of the pyrrole-to-OH ratio. It is interesting to note that the presence of hundreds of ppb of ozone in the reactor might also lead to additional production of OH through ozone photolysis, producing $O(^1D)$, which then quickly reacts with $H_2O$ to form two OH radicals. Therefore, OH radicals present in the reactor may not only come from $H_2O$ photolysis but also from $O_3$ photolysis.

### 5.3 Correction for not operating the CRM under pseudo-first-order conditions

Corrected values of C2 (Eq. ( 3 )) and C3 (Eq. ( 4)) are used in equation ( 1 ) to calculate the measured OH reactivity. As mentioned previously, Eq. ( 1 ) rests on the assumption that chemical reactions occur under first-order kinetic conditions with respects to pyrrole and ambient trace gases. However, as discussed above, this assumption is not fulfilled since the OH mixing ratio inside the reactor is on the same magnitude than the pyrrole mixing ratio. The correction applied to the calculated OH reactivity values to account for this artifact is described below.

#### 5.3.1 Experimental characterization - dependence on the pyrrole-to-OH ratio

Figure 6 displays experimental observations of the measurement bias caused by not operating the instrument under pseudo-first-order conditions. This figure compares OH reactivity values calculated from the addition of a gas standard to values measured by the MD-CRM instrument. The measurements were derived using equation ( 1) and corrected for changes in humidity between C2 and C3 (see section 5.1). NOx species were not added in these experiments.

The top panel of Figure 6 shows results from the addition of three different gas standards (isoprene, ethane, and propene), characterized by OH rate constants spanning almost 3 orders of magnitude ($1.0\ 10^{-10}$, $2.4\ 10^{-13}$, and $2.9\ 10^{-11}$ $cm^3$ $molecules^{-1}$ $s^{-1}$, respectively), at a pyrrole-to-OH ratio of 1.4. This figure indicates a linear relationship between the measured and the calculated OH reactivity values. The slope *F* of a linear

regression represents the correction factor that has to be applied to the measured OH reactivity values (see Eq. ( 8):

$$R_{OH}^{true} = F * R_{OH}^{measured} \quad (8)$$

Where $R_{OH}^{true}$ is the calculated total OH reactivity, based on the concentrations and OH reaction rate constants of the gas standards, and $R_{OH}^{measured}$ is the OH reactivity measured by the MD-CRM instrument, corrected for changes in relative humidity between C2 and C3. For ambient measurements, $R_{OH}^{true}$ will be the measured OH reactivity corrected for not operating the instrument under pseudo-first-order conditions.

The correction factors determined at a pyrrole-to-OH ratio of 1.4 indicate that the reactivity of the gas standard plays a role in the observed bias. Higher correction factors are found for more reactive compounds. Indeed, at a pyrrole-to-OH ratio of 1.4, the correction factor determined for isoprene is 7.6% higher than for propene and is 50.6% higher than for ethane. However, the middle panel of Fig. 6 indicates that the differences observed between the different gas standards are lower at a pyrrole-to-OH ratio of 2.3, with the correction factor derived for isoprene being only 1% different than for ethane.

Experiments performed at various pyrrole-to-OH ratios (4 ratios: 1.4, 1.6, 1.8, 2.3, not shown) indicate that the relative difference between the correction factors determined using ethane and isoprene range from 1-58% and confirms the strong dependence on the pyrrole-to-OH ratio, with negligible differences for ratios higher than 2.3. These two gas standards represent extreme cases since ethane is one of the less reactive VOCs in the atmosphere (reaction rate constant with OH: 2.4 $10^{-13}$ $cm^3$ $molecules^{-1}$ $s^{-1}$) while isoprene is one of the most reactive (reaction rate constant with OH: 1.0 $10^{-10}$ $cm^3$ $molecules^{-1}$ $s^{-1}$). It is interesting to note that ambient air is a mixture of a large number of compounds with reaction rate constants ranging between that of ethane and isoprene. The correction factor should therefore be calculated as an averaged correction factor determined using a VOC exhibiting a slow rate constant with OH such as ethane and a VOC exhibiting a fast rate constant such as isoprene. The uncertainty on the averaged correction factor can then be estimated from the difference observed in *F* for these 2 VOCs.

Results from the addition of the same gas standard (isoprene) at three different pyrrole-to-OH ratios (1.4, 1.8, and 2.3) are shown in the bottom panel of Figure 6. Correction factors derived from these experiments increase when the pyrrole-to-OH ratio decreases. Indeed, the highest correction factor (1.59) is found for the lowest pyrrole-to-OH ratio (i.e. 1.4) and the

lowest correction factor (0.84) is found for the highest Pyrrole-to-OH ratio (i.e. 2.3). A decrease of the correction factor with the pyrrole-to-OH ratio is consistent with a kinetic regime getting closer to pseudo-first-order conditions (OH<<Pyrrole) and therefore to correction factors closer to one.

Results from the addition of other gas standards (ethene, $k = 8{,}5\times10^{-12}$ $cm^3$ $molecules^{-1}$ $s^{-1}$, and propane, $k = 1.09\times10^{-12}$ $cm^3$ $molecules^{-1}$ $s^{-1}$) are consistent with the results shown in Fig. 6 and confirmed the trends discussed above (Fig. S7).

From these experiments, it appears essential to take into account the pyrrole-to-OH ratio in the correction to apply to the measured OH reactivity values. Figure 7 shows how the correction factor varies with the pyrrole-to-OH ratio. Correction factors shown in this figure were derived from single experiments using different standards (ethane, ethene, propane, propene, and isoprene) as shown in Figure 6. This figure gathers laboratory and field experiments performed over 7 months. The gas standards were chosen to cover a large range of reaction rate constants with OH (from 2.4 $10^{-13}$ $cm^3$ $molecules^{-1}$ $s^{-1}$ for ethane to 1.0 $10^{-10}$ $cm^3$ $molecules^{-1}$ $s^{-1}$ for isoprene) to take into account the impact of the gas reactivity on the correction factor.

From the linear relationship observed in Figure 7, the correction factor to apply to the measurements can be calculated using eq. (9) and the pyrrole-to-OH ratio that is monitored during field or laboratory measurements.

$$F = -0.16\,Pyr/OH + 1.27 \quad (9)$$

Within the small range of pyrrole-to-OH ratios generally encountered during field campaigns, typically from 1.6 to 2.2, the correction factors determined using Eq. (9) range between 0.9 and 1.0. Therefore, an averaged value of the correction factors can be considered instead of using a pyrrole-to-OH dependent correction (Figure 7). It is interesting to note that this correction takes into account the artifact caused by not operating the instrument under pseudo-first-order conditions but also any unknown artifact that could impact the OH reactivity measurements, such as radical segregation and wall losses of radicals inside the reactor.

### 5.3.2 Comparison of model simulations to laboratory observations

Simulations performed using both mechanisms described in section 3 (the simple mechanism and MCM), as well as a mechanism similar to the one described by Sinha et al.

(2008), which does not account for radical-radical reactions, are displayed in Figure 8. The latter is referred as 2-reaction mechanism in the following.

The top panel of Figure 8 displays the results from the addition of three different gas standards (isoprene, ethane, and propene) using the MCM mechanism and a surrogate standard for the simple mechanism, characterized by different reaction rate constants with OH ($1.0\ 10^{-10}$, $2.4\ 10^{-13}$, $2.9\ 10^{-11}$, and $5.0\ 10^{-12}$ $cm^3$ $molecules^{-1}$ $s^{-1}$, respectively). These simulations were performed at a pyrrole-to-OH ratio of 1.4. It is interesting to note that simulations performed using MCM for a gas standard exhibiting an OH rate constant of $5.0\ 10^{-12}$ $cm^3$ $molecules^{-1}$ $s^{-1}$ are similar to that observed with the simple mechanism, suggesting that the detailed secondary chemistry included in MCM is not important to model this correction. These results show that the correction factor should increase with the OH rate constant, independently of the mechanism used (the MCM or the simple mechanism). This trend is consistent with laboratory observations discussed above.

Simulations conducted with the simple mechanism and the 2-reaction mechanism are displayed in the bottom panel of Figure 8 for a surrogate gas standard ($k = 5.0\ 10^{-12}$ $cm^3$ $molecules^{-1}$ $s^{-1}$) at three different pyrrole-to-OH ratios (1.4, 1.9, and 2.9). The correction factor derived with the simple mechanism decreases with increasing pyrrole-to-OH ratios as observed during the laboratory experiments. As mentioned previously, these observations are consistent with a chemical system getting closer to pseudo-first-order conditions (OH<<Pyrrole) when the pyrrole-to-OH ratio increases. In contrast, an opposite trend is observed when the 2-reaction mechanism is used. This result highlights the importance of accounting for radical-radical reactions in the mechanism to describe the complex chemistry occurring in the reactor. Both mechanisms, the simple mechanism and MCM, lead to correction factors that are converging to unity when pyrrole-to-OH increases (i.e. OH decreases).

Figure 9 (Top panel) shows how the correction factor changes with the pyrrole-to-OH ratio. Simulated values stem from simulations conducted using the box model including the MCM mechanism and constrained with ethane or isoprene under dry conditions, as well as under wet conditions (RH = 100%) for ethane. The simulated correction factors for ethane under dry conditions are higher than the measurements by 72% and 54% at pyrrole-to-OH ratios of 1.4 and 1.9, respectively. These differences are even larger for isoprene (143% and 80% at pyrrole-to-OH ratios of 1.4 and 1.9, respectively). However, a similar trend is observed: i.e. a decrease of the correction factors with increasing pyrrole-to-OH ratios. Performing simulations at 100% of relative humidity improves the agreement but still fails

short to reconcile simulations and measurements. Furthermore, a RH of 100% is not likely inside the reactor, and the real conditions are between these two extreme cases.

Several hypotheses (segregation between the reactants, $RO_2$+OH reactions (Fittschen et al., 2014), uncertainties in reaction rate constants of radical-radical reactions, higher or lower proportions of $HO_2$ compared to OH, formation of $O_3$ inside the reactor) were tested in the simulations to try to reconcile simulated results and laboratory observations (see supplementary material S8 to S13). Unfortunately, none of these hypotheses seems to fully explain the disagreement, even if accounting for (i) uncertainties in reaction rate constants of radical-radical reactions and (ii) a potential lower proportion of $HO_2$ compared to OH allow improving the agreement. The combination of these two hypotheses (lower proportion of $HO_2$ by 25% and reaction rate constants of OH + $HO_2$ reduced by 20%) leads to an agreement within 15% (not shown).

The model inability to reproduce laboratory observations may be due to (i) the approach used to perform the simulations (see section 3), (ii) a misrepresentation of the secondary chemistry for pyrrole, and (iii) an impact of the flow dynamic inside the reactor. Improving model simulations would require to investigate the pyrrole chemistry, to couple the chemical mechanisms to a CFD (Computational Fluid Dynamics) model, and to consider that a constant production of OH from the injector would lead to the reaction of OH with byproducts and peroxy radicals previously formed inside the reactor.

Nevertheless, similar behaviors observed between simulations and experiments give confidence in experimentally-derived correction factors. It is worth noting that the dependence of $F$ on the reactivity of added gas standards is reduced at higher pyrrole-to-OH ratios (see Figure 9, bottom panel). A similar trend is observed for the water dependence. It would therefore be beneficial to run the CRM instruments at high pyrrole-to-OH ratios to reduce the uncertainty introduced by the correction applied to account for not operating the instrument under pseudo-first-order conditions, keeping in mind that a higher pyrrole-to-OH ratio leads to a lower OH mixing ratio in the reactor, which in turn worsen the detection limit. Working at pyrrole-to-OH ratios ranging from 1.7-2.0 seems to be optimal for the MD-CRM instrument.

### 5.4 Detection limit and measurement uncertainties

The detection limit (LOD) indicates the minimal detectable difference between C2 and C3. The LOD was determined keeping the CRM instrument under C2 conditions for 15 hours

during the Dunkirk field campaign (see section 4). This 15 hours segment was then split into 5-min subsets to calculate a standard deviation ($\sigma_{C2}$) for each subset and an averaged value of the standard deviation for the whole time period ($\overline{\sigma_{C2}}$). This approach was used to avoid the variability in C2 measurements due to changes in ambient relative humidity, which drives the zero air humidity. An OH reactivity value was then calculated using the measured C1 value, an averaged C2 value ($\overline{C2}$), and 3 times the average standard deviation calculated above (i.e. $C3 = \overline{C2} + 3\overline{\sigma_{C2}}$). The calculated OH reactivity value, characteristic of the LOD at 3σ, was 3.0 $s^{-1}$ for an averaged pyrrole-to-OH ratio of 1.7.

To assess the total uncertainty of the OH reactivity measurements, we need to consider a propagation of uncertainties from all the parameters included in the OH reactivity calculation (Eq. ( 1)), including all the corrections described in this publication. A detailed description of this approach is given in the supplementary material (section S14).

An example of precision values (random error) and total uncertainty values, taking into account different levels of corrections, is given as a function of total OH reactivity measurements in Figure 10 (top panel) for the Dunkirk field campaign.

The precision (purple dots in the Top panel) is dependent on the OH reactivity level and ranges from approximately 50% at the LOD of 3 $s^{-1}$ to less than 4% at OH reactivity values higher than 50 $s^{-1}$. When systematic errors, except those associated to the humidity and NO corrections, are accounted for in the total uncertainty calculation (blue dots), the total uncertainty levels off at approximately 17.5% for OH reactivity values higher than 15 $s^{-1}$, while a low impact is observed at lower OH reactivity values. This is consistent with the systematic errors and the measurement precision driving the uncertainty at high and low OH reactivity levels, respectively.

Including uncertainties due to the correction for humidity changes between C2 and C3 (green open dots) has a small impact on the total uncertainty and only small differences are observed (1.5±3.0% of relative differences on average). Finally, including uncertainties due to the correction for NO interferences (red open dots) leads to a sharp increase of the total uncertainty for data points characterized by elevated NO mixing ratios (7.3±39.8% of relative differences on average).

Figure 10 (bottom panel), shows the total uncertainty, including all sources of errors (precision, systematic errors, corrections), as a function of total OH reactivity and color-coded by $NO_x$ levels. The largest uncertainties are found for high $NO_x$ levels (from 20 to 120 ppb). The total uncertainty for OH reactivity values higher than 15 $s^{-1}$ depends strongly on NO and

ranges from 18-25% at $NO_x$ mixing ratios < 30 ppb; 25-70% at $NO_x$ mixing ratios of 30-80 ppb; and can be as high as 200% at $NO_x$ levels above 80 ppb, depending on the total OH reactivity level.

Time series of ambient OH reactivity measurements at different stages of the data processing are presented in Figure 11 for the Dunkirk field campaign, showing the amplitudes of the different corrections.

In urban environments such as the Dunkirk site, the correction for $NO_x$ has the largest impact on OH reactivity measurements and is 9.2±15.7 $s^{-1}$ on average. The correction that has the second largest impact is due to not operating the instrument under pseudo-first-order conditions and is 8.5±5.8 $s^{-1}$ on average. The humidity correction is also significant and is 5.2±3.2 $s^{-1}$ on average due to fast changes in ambient RH (proximity of the sea). The correction for dilution is constant and leads to an increase of the measurements by a factor 1.23. It is interesting to note that the accuracy of this approach to correct the OH reactivity measurements on the MD-CRM instrument has been tested in Hansen et al. (2015) and has been found to be suitable for $NO_x$ mixing ratios up to 70-100 ppbv.

## Conclusion

This study presents the results of an exhaustive characterization of a CRM instrument developed at Mines Douai. This characterization aimed at assessing the different corrections that need to be applied on the OH reactivity measurements and to evaluate our understanding of the chemical processes occurring inside the CRM reactor. A suite of laboratory experiments was conducted and the results were compared to simulations from a box model including a simple chemical mechanism made of 42 reactions and a more exhaustive chemical mechanism based on a subset of the Master Chemical Mechanism (MCM). The latter was made of 1610 reactions.

As previously reported in the literature, artifacts in total OH reactivity measurements were identified from (i) changes in humidity between C2 and C3 measurements, (ii) the spurious formation of OH through the $HO_2$ + NO reaction, and (iii) not operating the instrument under pseudo-first-order conditions. The correction to apply for (i) can easily be assessed by monitoring the dependence of C2 with a proxy for humidity, e.g. m37/m19 on PTR-MS instruments.

A quadratic parameterization was developed to correct the OH reactivity measurements for (ii) by characterizing the sensitivity of C3 to NO and to the Pyrrole-to-OH

ratio. Changes in C3 levels were found to increase and to level off with NO concentrations and to increase with the pyrrole-to-OH ratio. C3 was also found to be sensitive to $NO_2$. This dependence was attributed to a conversion of $NO_2$ into NO of approximately 24%, occurring mainly on surfaces and not due to photolysis in the reactor. This unwanted conversion will be carefully investigated in future studies to eliminate it or to reduce it at a negligible level.

The correction to apply for (iii) was assessed by adding trace gases inside the reactor and by comparing the measured OH reactivity to expected values. These gases were chosen to exhibit different reaction rate constants with OH and experiments were performed at different pyrrole-to-OH ratios. Dependences of the correction factor on the bimolecular rate constant and on the pyrrole-to-OH ratio were observed experimentally. We recommend using an average correction factor derived from experiments made using at least two different standards, the first one exhibiting a slow rate constant with OH, such as ethane, and the second one exhibiting a fast rate constant, such as isoprene. It is also recommended to develop a parameterization depending on the Pyrrole-to-OH ratio if a large range of ratios is observed during ambient measurements.

Model simulations reproduced the magnitude of the main corrections as well as their dependences on the Pyrrole-to-OH ratio and the rate constant of the gas standard. The reasonable agreement observed between simulations and experiments give confidence in the parameterizations proposed in this study. However, it would be hazardous to use the numerical values of these parameterizations for other CRM instruments and it is recommended that each group characterizes its own instrument. It is interesting to note that a comparison of the corrections needed on different CRM instruments would help investigating the robustness of this technique.

However, some differences were observed between simulations and experimental results, pointing out the need for a better understanding of the pyrrole chemistry. Additional work is needed to investigate its oxidation chemistry. In addition, it would be worth coupling a CFD model to the chemical mechanisms described in this work to investigate the impact of flow dynamics on the CRM measurements, which in turn would provide a better description of the complex processes occurring in the reactor.

The CRM instrument developed at Mines Douai has already been successfully deployed in the field and has given satisfactory results in different environments. Good agreements during intercomparison exercises with other instruments, another CRM instrument and a Pump-Probe instrument, have been found, highlighting the suitability of the proposed corrections for the CRM technique.

## Acknowledgement

The authors are grateful to Prof. J. Williams (MPIC-Mainz) for providing a CRM glass reactor, Dr. V. Sinha (IISER-Mohali) for his assistance during the development of the MD-CRM instrument, and Dr. Stephane Sauvage for helpful discussions about the assessment of measurement uncertainties. This research was funded by the European Union Seventh Framework Programme under Grant Agreement number 293897, "DEFIVOC" project and by the CaPPA project. The CaPPA project (Chemical and Physical Properties of the Atmosphere) is funded by the French National Research Agency (ANR) through the PIA (Programme d'Investissement d'Avenir) under contract "ANR-11-LABX-0005-01" and by the Regional Council Nord-Pas de Calais and the "European Funds for Regional Economic Development" (FEDER). R. F. Hansen's internship in Mines Douai was supported by a Chateaubriand Science Fellowship from the French Embassy of the United States. The authors also want to thank all colleagues involved in the field deployments of the MD-CRM instrument.

## References


Atkinson, R., Aschmann, S. M., Winer, A. M. and Carter, W. P. L.: Rate constants for the gas phase reactions of OH radicals and $O_3$ with pyrrole at 295 ± 1 K and atmospheric pressure, Atmos. Environ. 1967, 18(10), 2105–2107, doi:10.1016/0004-6981(84)90196-3, 1984.

Bloss, C., Wagner, V., Jenkin, M. E., Volkamer, R., Bloss, W. J., Lee, J. D., Heard, D. E., Wirtz, K., Martin-Reviejo, M., Rea, G., Wenger, J. C., and Pilling, M. J.: Development of a detailed chemical mechanism (MCMv3.1) for the atmospheric oxidation of aromatic hydrocarbons, Atmos. Chem. Phys., 5, 641–664, doi:10.5194/acp-5-641-2005, 2005.

Calpini, B., Jeanneret, F., Bourqui, M., Clappier, A., Vajtai, R. and van den Bergh, H.: Direct measurement of the total reaction rate of OH in the atmosphere, Analusis, 27(4), 328–336, doi:10.1051/analusis:1999270328, 1999.

Carslaw, N., Creasey, D. J., Heard, D. E., Jacobs, P. J., Lee, J. D., Lewis, A. C., McQuaid, J. B., Pilling, M. J., Bauguitte, S., Penkett, S. A., Monks, P. S., and Salisbury, G.: Eastern Atlantic Spring Experiment 1997 (EASE97) – 2. Comparisons of model concentrations of OH, $HO_2$, and $RO_2$ with measurements, J. Geophys. Res., 107, D14, 4190, 2002.

De Gouw, J. and Warneke, C.: Measurements of volatile organic compounds in the Earth's atmosphere using proton-transfer reaction mass spectrometry, Mass Spectrom. Rev., 26, 223–257, 2007.

Di Carlo, P., Brune, W. H., Martinez, M., Harder, H., Lesher, R., Ren, X., Thornberry, T., Carroll, M. A., Young, V., Shepson, P. B., Riemer, D., Apel, E., and Campbell, C.: Missing OH Reactivity in a Forest: Evidence for Unknown Reactive Biogenic VOCs, Science, 304, 722–725, doi:10.1126/science.1094392, 2004.

Dillon, T., Tucceri, M., Dulitz, K., Horowitz, A., Vereecken, L., and Crowley, J.: Reaction of Hydroxyl Radicals with $C_4H_5N$ (Pyrrole): Temperature and Pressure Dependent Rate Coefficients, J. Phys. Chem. A, 116, 6051–6058, doi:10.1021/jp211241x, 2012.

Dolgorouky, C., Gros, V., Sarda-Esteve, R., Sinha, V., Williams, J., Marchand, N., Sauvage, S., Poulain, L., Sciare, J. and Bonsang, B.: Total OH reactivity measurements in Paris during the 2010 MEGAPOLI winter campaign, Atmos. Chem. Phys., 12(20), 9593–9612, doi:10.5194/acp-12-9593-2012, 2012.

Dusanter, S., Vimal, D., Stevens, P. S., Volkamer, R., Molina, L. T., Baker, A., Meinardi, S., Blake, D., Sheehy, P., Merten, A., Zhang, R., Zheng, J., Fortner, E. C., Junkermann, W., Dubey, M., Rahn, T., Eichinger, B., Lewandowski, P., Prueger, J., and Holder, H.: Measurements of OH and $HO_2$ concentrations during the MCMA-2006 field campaign – Part 2: Model comparison and radical budget, Atmos. Chem. Phys., 9, 6655–6675, doi:10.5194/acp-9-6655-2009, 2009.

Edwards, P. M., Evans, M. J., Furneaux, K. L., Hopkins, J., Ingham, T., Jones, C., Lee, J. D., Lewis, A. C., Moller, S. J., Stone, D., Whalley, L. K., and Heard, D. E.: OH reactivity in a South East Asian tropical rainforest during the Oxidant and Particle Photochemical Processes (OP3) project, Atmos. Chem. Phys., 13, 9497–9514, doi:10.5194/acp-13-9497-2013, 2013.

Fittschen, C., Whalley, L. K., Heard, D. E.: The Reaction of $CH_3O_2$ Radicals with OH Radicals: A Neglected Sink for $CH_3O_2$ in the Remote Atmosphere, Environ. Sci. Technol., 48, 14, 7700-7701, 2014

Goldstein, A. H. and Galbally, I. E.: Known and unexplored organic constituents in the earth's atmosphere, Environ. Sci. Technol., 41, 1514–1521, 2007

Hansen, R. F., Griffith, S. M., Dusanter, S., Rickly, P. S., Stevens, P. S., Bertman, S. B., Carroll, M. A., Erickson, M. H., Flynn, J. H., Grossberg, N., Jobson, B. T., Lefer, B. L., and Wallace, H. W.: Measurements of total hydroxyl radical reactivity during CABINEX 2009 – Part 1: field measurements, Atmos. Chem. Phys., 14, 2923-2937, doi:10.5194/acp-14-2923-2014, 2014.

Hansen, R. F., Blocquet, M., Schoemaecker, C., Léonardis, T., Locoge, N., Fittschen, C., Hanoune, B., Stevens, P. S., Sinha, V., and Dusanter, S.: Intercomparison of the comparative reactivity method (CRM) and pump-probe technique for measuring total OH reactivity in an urban environment, Atmos. Meas. Tech. Discuss., 8, 6119-6178, doi:10.5194/amtd-8-6119-2015, 2015

Hofzumahaus, A., Rohrer, F., Lu, K. D., Bohn, B., Brauers, T., Chang, C. C., Fuchs, H., Holland, F., Kita, K., Kondo, Y., Li, X., Lou, S. R., Shao, M., Zeng, L. M., Wahner, A., and Zhang, Y. H.: Amplified Trace Gas Removal in the Troposphere, Science, 324, 1702–1704, 2009.

Jenkin, M. E., Saunders, S. M., and Pilling, M. J.: The tropospheric degradation of volatile organic compounds: a protocol for mechanism development, Atmos. Environ., 31, 81–104, 1997.

Jenkin, M. E., Saunders, S. M., Wagner, V., and Pilling, M. J.: Protocol for the development of the Master Chemical Mechanism, MCM v3 (Part B): tropospheric degradation of aromatic volatile organic compounds, Atmos. Chem. Phys., 3, 181–193, doi:10.5194/acp-3-181-2003, 2003.

Jenkin, M. E., Wyche, K. P., Evans, C. J., Carr, T., Monks, P. S., Alfarra, M. R., Barley, M. H., McFiggans, G. B., Young, J. C., and Rickard, A. R.: Development and chamber evaluation of the MCM v3.2 degradation scheme for β-caryophyllene, Atmos. Chem. Phys., 12, 5275–5308, doi:10.5194/acp-12-5275-2012, 2012.

Kim, S., Guenther, A., Karl, T. and Greenberg, J.: Contributions of primary and secondary biogenic VOC to total OH reactivity during the CABINEX (Community Atmosphere-Biosphere INteractions Experiments)-09 field campaign, Atmos Chem Phys, 11(16), 8613–8623, doi:10.5194/acp-11-8613-2011, 2011

Kovacs, T. A. and Brune, W. H.: Total OH Loss Rate Measurement, J. Atmos. Chem., 39(2), 105–122, doi:10.1023/A:1010614113786, 2001.

Levy, H.: Photochemistry of the lower troposphere, Planet. Space. Sci, 20, 919–935, 1972.

Lou, S., Holland, F., Rohrer, F., Lu, K., Bohn, B., Brauers, T., Chang, C., Fuchs, H., Häseler, R., Kita, K., Kondo, Y., Li, X., Shao, M., Zeng, L., Wahner, A., Zhang, Y., Wang, W., and Hofzumahaus, A.: Atmospheric OH reactivities in the Pearl River Delta – China in summer

2006: measurement and model results, Atmos. Chem. Phys., 10, 11243–11260, doi:10.5194/acp-10-11243-2010, 2010.

Martinez, M., Harder, H., Kovacs, T. A., Simpas, J. B., Bassis, J., Lesher, R., Brune, W. H., Frost, G. J., Williams, E. J., Stroud, C. A., Jobson, B. T., Roberts, J. M., Hall, S. R., Shetter, R. E., Wert, B., Fried, A., Alicke, B., Stutz, J., Young, V. L., White, A. B., and Zamora, R. J.: OH and $HO_2$ concentrations, sources, and loss rates during the Southern Oxidants Study in Nashville, Tennessee, summer 1999, J. Geophys. Res., 108, D19, 4617, 2003.

Michoud, V., Kukui, A., Camredon, M., Colomb, A., Borbon, A., Miet, K., Aumont, B., Beekmann, M., Durand-Jolibois, R., Perrier, S., Zapf, P., Siour, G., Ait-Helal, W., Locoge, N., Sauvage, S., Afif, C., Gros, V., Furger, M., Ancellet, G., and Doussin, J. F.: Radical budget analysis in a suburban European site during the MEGAPOLI summer field campaign, Atmos. Chem. Phys., 12, 11951–11974, doi:10.5194/acp-12-11951-2012, 2012.

Nölscher, A. C., Williams, J., Sinha, V., Custer, T., Song, W., Johnson, A. M., Axinte, R., Bozem, H., Fischer, H., Pouvesle, N., Phillips, G., Crowley, J. N., Rantala, P., Rinne, J., Kulmala, M., Gonzales, D., Valverde-Canossa, J., Vogel, A., Hoffmann, T., Ouwersloot, H. G., Vilà-Guerau de Arellano, J. and Lelieveld, J.: Summertime total OH reactivity measurements from boreal forest during HUMPPA-COPEC 2010, Atmos. Chem. Phys., 12(17), 8257–8270, doi:10.5194/acp-12-8257-2012, 2012a.

Nölscher, A. C., Sinha, V., Bockisch, S., Klüpfel, T. and Williams, J.: Total OH reactivity measurements using a new fast Gas Chromatographic Photo-Ionization Detector (GC-PID), Atmos. Meas. Tech., 5(12), 2981–2992, doi:10.5194/amt-5-2981-2012, 2012b.

Nölscher, A. C., Bourtsoukidis, E., Bonn, B., Kesselmeier, J., Lelieveld, J. and Williams, J.: Seasonal measurements of total OH reactivity emission rates from Norway spruce in 2011, Biogeosciences, 10(6), 4241–4257, doi:10.5194/bg-10-4241-2013, 2013.

Nölscher, A. C.; Butler, T.; Auld, J.; Veres, P.; Munoz, A.; Taraborrelli, D.; Vereecken, L.; Lelieveld, J.; Williams, J.: Using total OH reactivity to assess isoprene photooxidation via measurement and model, Atmos. Environ., 89, 453-463, 2014

Sadanaga, Y., Yoshino, A., Watanabe, K., Yoshioka, A., Wakazono, Y., Kanaya, Y., and Kajii, Y.: Development of a Measurement System of OH reactivity in the atmosphere by using a laser-induced pump and probe technique, Rev. Sci. Instrum., 75, 2648-2655, 2004.

Saunders, S. M., Jenkin, M. E., Derwent, R. G., and Pilling, M. J.: Protocol for the development of the Master Chemical Mechanism, MCM v3 (Part A): tropospheric degradation of non-aromatic volatile organic compounds, Atmos. Chem. Phys., 3, 161–180, doi:10.5194/acp-3-161-2003, 2003.

Sinha, V., Williams, J., Crowley, J. N. and Lelieveld, J.: The Comparative Reactivity Method – a new tool to measure total OH Reactivity in ambient air, Atmos. Chem. Phys., 8(8), 2213–2227, doi:10.5194/acp-8-2213-2008, 2008.

Sinha, V., Williams, J., Lelieveld, J., Ruuskanen, T. M., Kajos, M. K., Patokoski, J., Hellen, H., Hakola, H., Mogensen, D., Boy, M., Rinne, J. and Kulmala, M.: OH Reactivity Measurements within a Boreal Forest: Evidence for Unknown Reactive Emissions, Environ. Sci. Technol., 44(17), 6614–6620, doi:10.1021/es101780b, 2010.

Sinha, V., Williams, J., Diesch, J. M., Drewnick, F., Martinez, M., Harder, H., Regelin, E., Kubistin, D., Bozem, H., Hosaynali-Beygi, Z., Fischer, H., Andrés-Hernández, M. D., Kartal, D., Adame, J. A. and Lelieveld, J.: Constraints on instantaneous ozone production rates and regimes during DOMINO derived using in-situ OH reactivity measurements, Atmos. Chem. Phys., 12(15), 7269–7283, doi:10.5194/acp-12-7269-2012, 2012.

Stone, D., Whalley, L. K., and Heard, D. E.: Tropospheric OH and $HO_2$ radicals: field measurements and model comparisons, Chem. Soc. Rev., 41, 6348–6404, 2012.

Whalley, L. K., Edwards, P. M., Furneaux, K. L., Goddard, A., Ingham, T., Evans, M. J., Stone, D., Hopkins, J. R., Jones, C. E., Karunaharan, A., Lee, J. D., Lewis, A. C., Monks, P. S., Moller, S. J., and Heard, D. E.: Quantifying the magnitude of a missing hydroxyl radical source in a tropical rainforest, Atmos. Chem. Phys., 11, 7223-7233, doi:10.5194/acp-11-7223-2011, 2011.

Zannoni, N., Dusanter, S., Gros, V., Sarda Esteve, R., Michoud, V., Sinha, V., Locoge, N., and Bonsang, B.: Intercomparison of two Comparative Reactivity Method instruments in the Mediterranean basin during summer 2013, Atmos. Meas. Tech. Discuss., 8, 5065-5104, doi:10.5194/amtd-8-5065-2015, 2015.

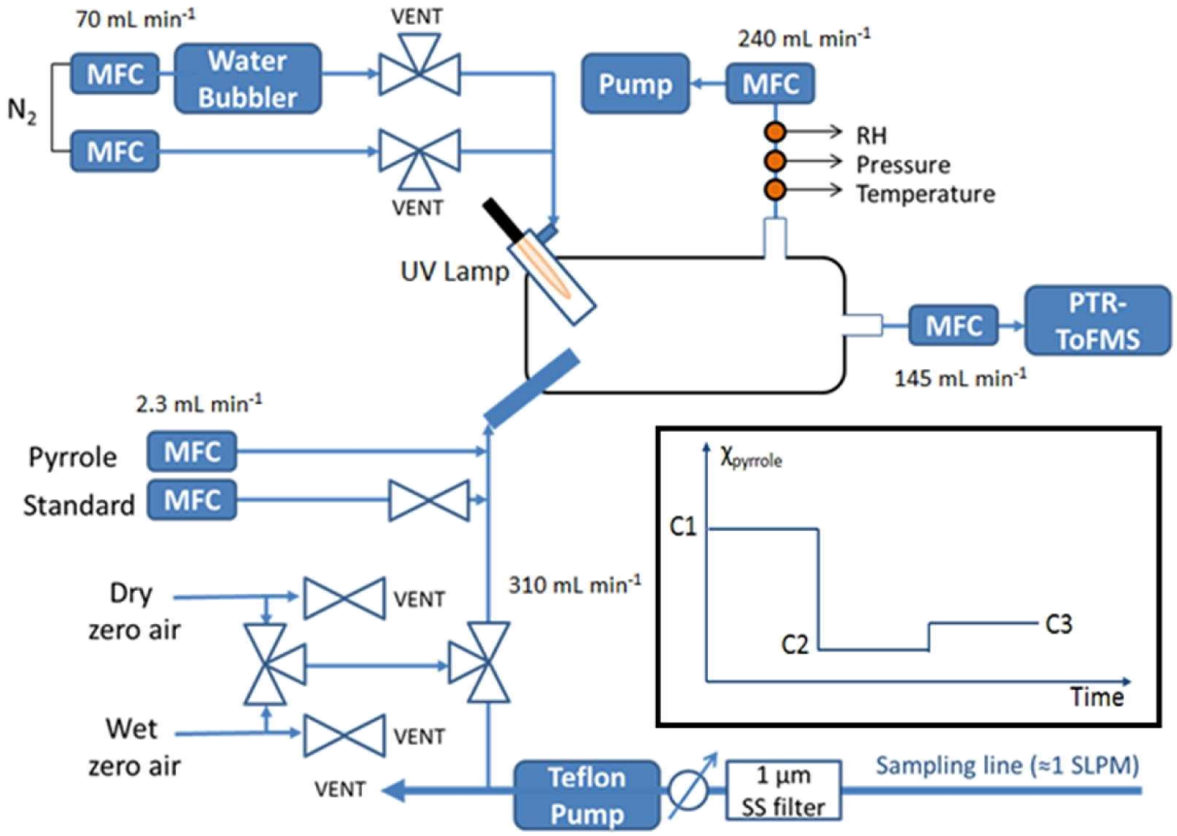


Figure 1 : Schematic of the Comparative Reactivity Method instrument developed at Mines Douai. Flow rates of different gases injected inside the CRM reactor (Pyrrole, $N_2$, air) or extracted from the reactor (PTR-MS sampling, reactor exhaust) are shown. The insert displays the measurement sequence for pyrrole (C1, C2, C3) during OH reactivity measurements.

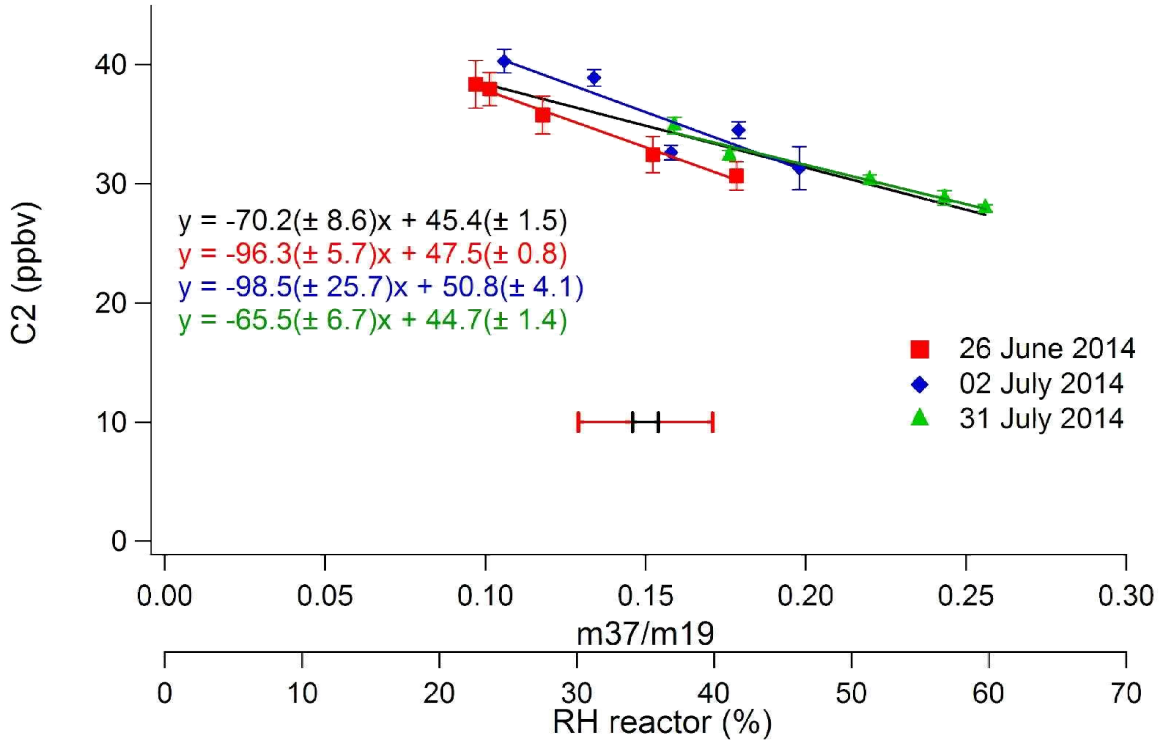


Figure 2 : Changes in C2 due to changes in RH. RH is tracked using the m37/m19 ratio monitored by PTR-ToFMS. The corresponding RH measured in the CRM reactor at 22°C is given on a second x-axis. Three experiments conducted during the Dunkirk field campaign are shown. The solid black line is a linear regression for the three experiments. Red, Blue, and green lines are linear regressions for individual experiments made on 26 June, 2 July, and 31 July, respectively. Error bars are the measurement precision (1σ). Black and red intervals are the mean and the maximum variations of m37/m19 observed between C2 and C3 during the Dunkirk campaign, respectively.

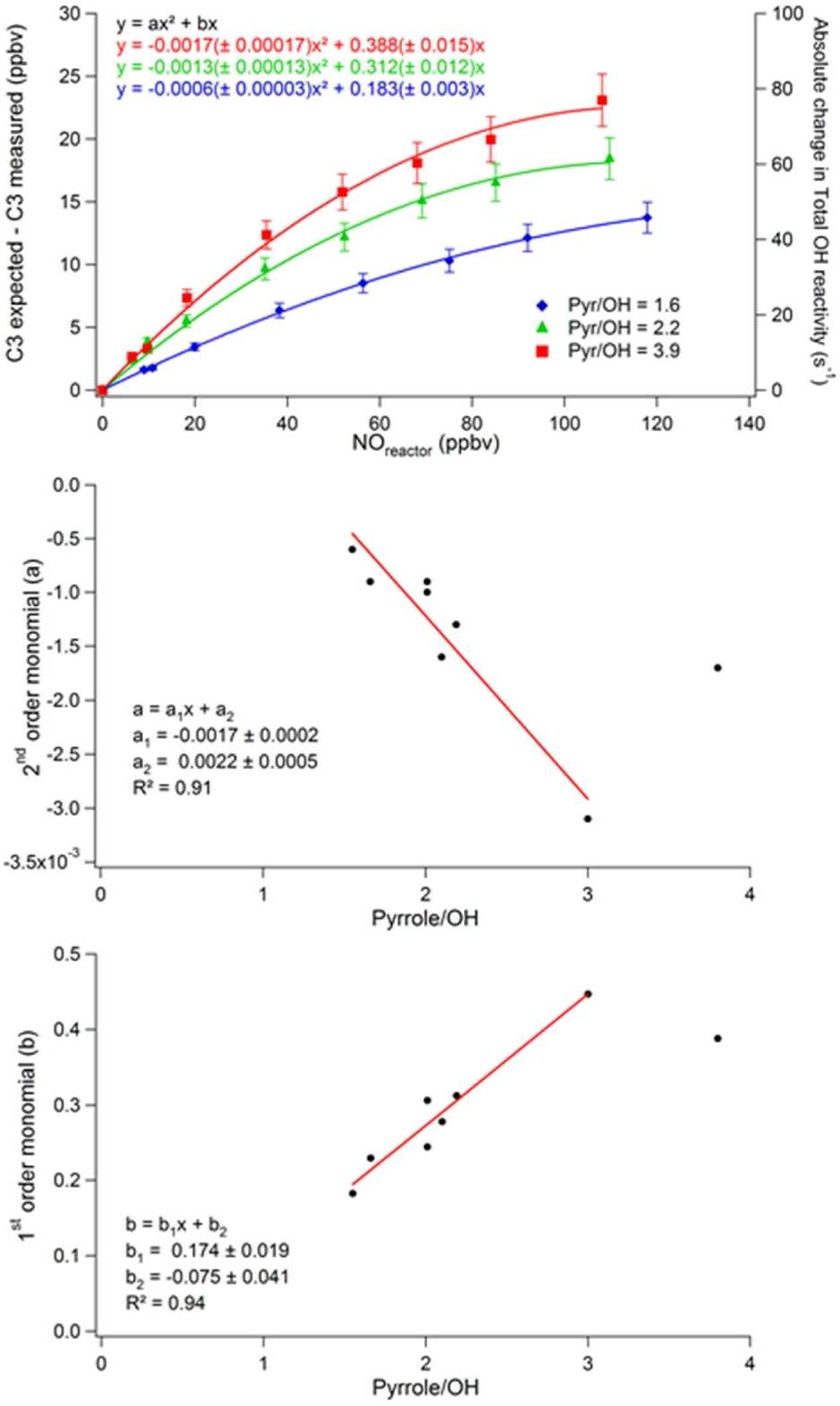


Figure 3 : Experimental parameterization of the NO artifact. Top panel left axis: Changes in C3 (ΔC3 = C3 expected – C3 measured) as a function of NO in the CRM reactor. Three experiments conducted at Pyrrole-to-OH ratios of 1.6 (blue diamonds), 2.2 (green triangles), and 3.9 (red squares) are shown. The right axis corresponds to absolute changes in total OH reactivity for the experiment conducted at a pyrrole-to-OH ratio of 2.2. Solid lines are quadratic regressions, whose equations are shown. Error bars are uncertainties on ΔC3

(approximately 9%) calculated by a quadratic propagation of errors. Middle and bottom Panels: Trends of the 1$^{st}$ (bottom) and 2$^{nd}$ (middle) order monomials with the pyrrole-to-OH ratio for the quadratic regressions displayed in the top panel. The experiment performed using dry zero air (Pyrrole-to-OH ratio of 3.9) is not included in the linear regressions (see text).

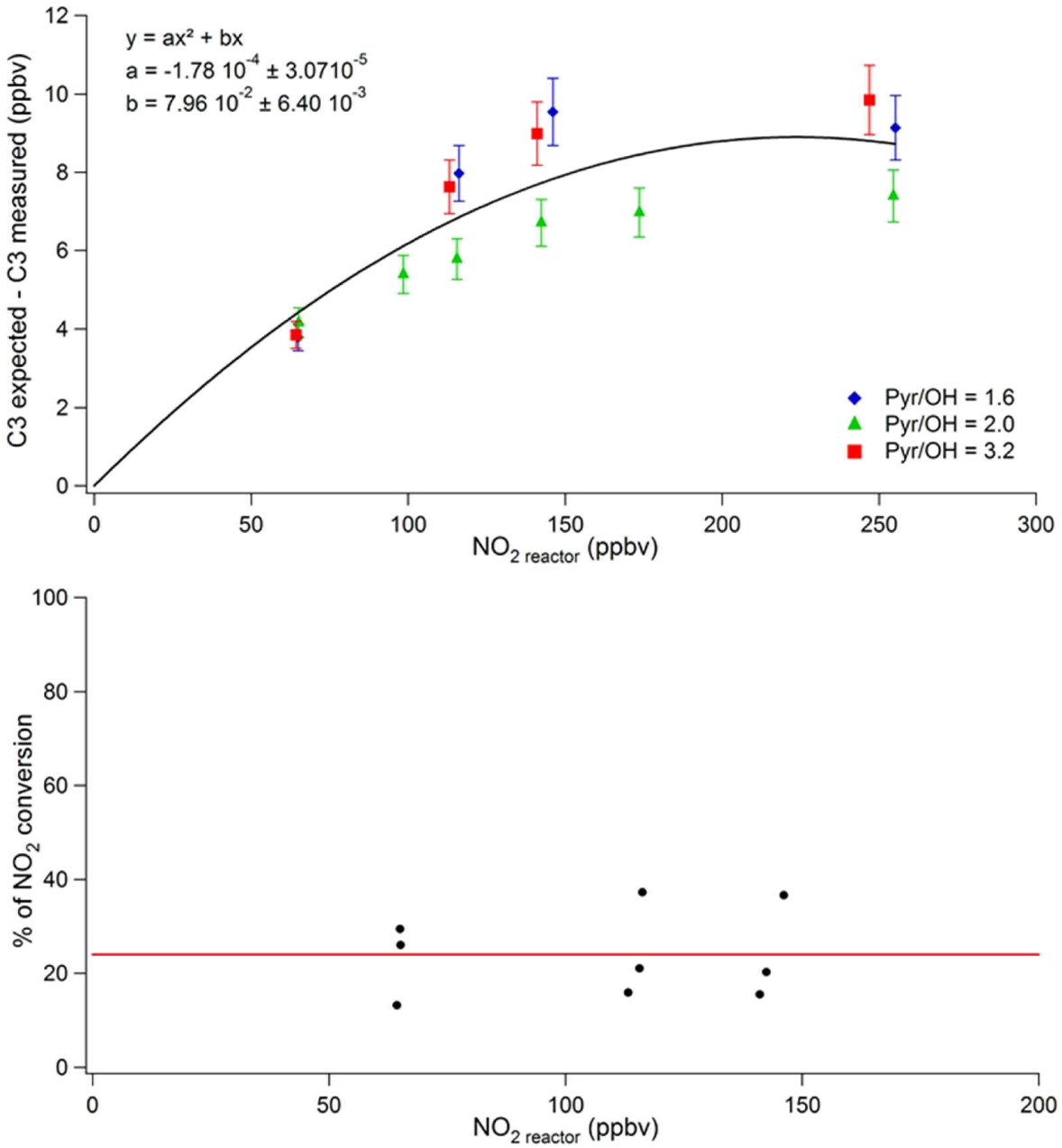


Figure 4 : Experimental parameterization of the $NO_2$ artifact. Top panel: Changes in C3 (ΔC3 = C3 expected – C3 measured) as a function of $NO_2$ in the CRM reactor. Three experiments conducted at Pyrrole-to-OH ratios of 1.6 (blue diamonds), 2.0 (green triangles), and 3.2 (red squares) are shown. Error bars are uncertainties on ΔC3 (approximately 9%) calculated by a quadratic propagation of errors. The black line and the equation correspond to a quadratic regression for the three experiments. Bottom panel: Quantification of the $NO_2$ fraction converted into NO (see text). The red line is the mean value of approximately 24% derived for the $NO_2$ conversion.

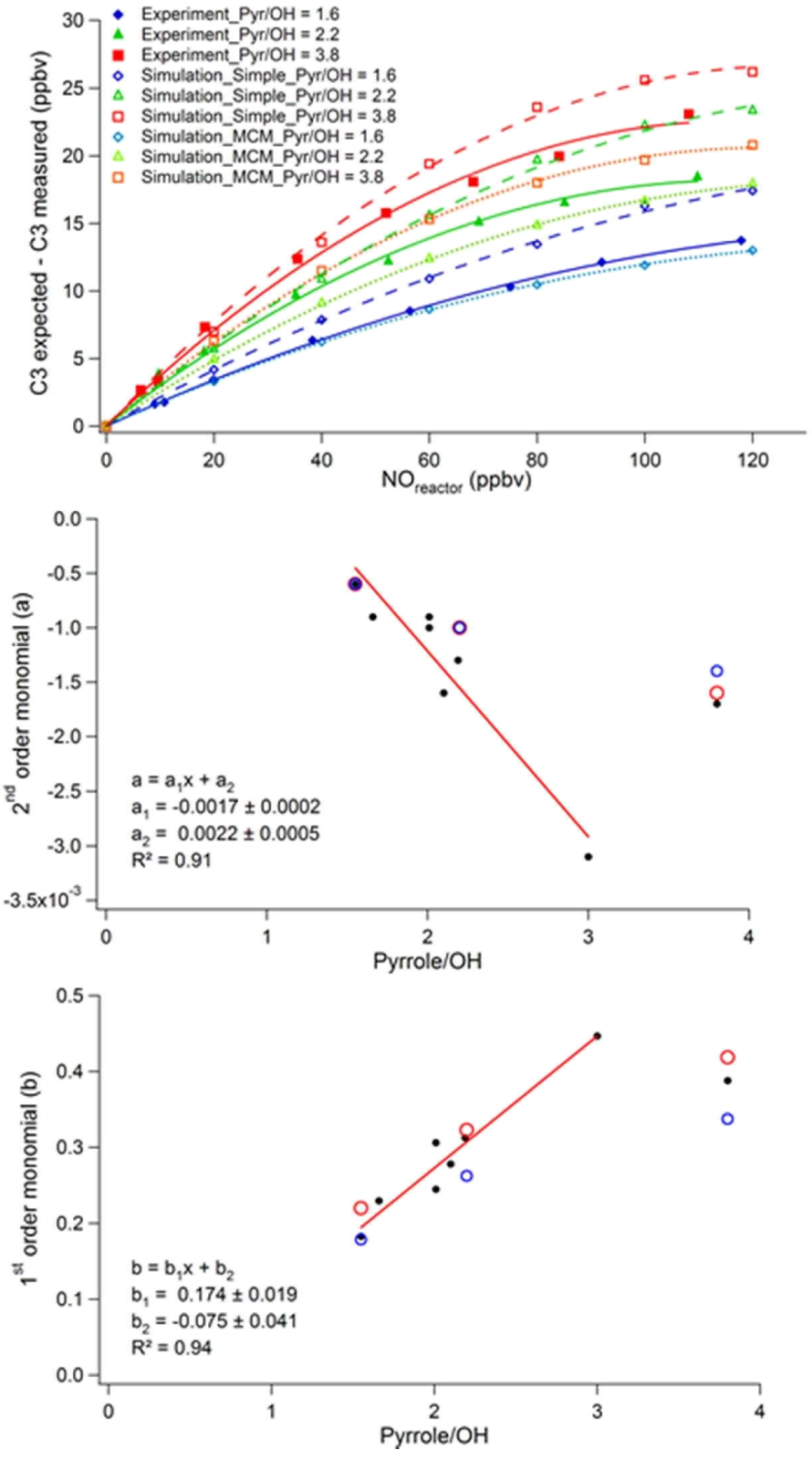


Figure 5: Comparison of model simulations to laboratory observations for the NO artifact. Top panel: Experimental (filled symbols and solid lines) and simulated (open symbols) results. The dashed and dotted lines are for the Simple Mechanism and MCM, respectively. Changes in C3 (ΔC3 = C3 expected – C3 measured) are shown as a function of NO in the CRM reactor. Experimental values are the same than in Figure 3. Simulations were made at the same Pyrrole-to-OH ratios than the experiments (same color code) and under dry

conditions. Middle and bottom Panel: Experimental (black dots) and simulated (open circles) results. Red and blue circles are for the simple mechanism and MCM, respectively. These curves show the trends of the 1$^{st}$ (bottom) and 2$^{nd}$ (middle) order monomials with the pyrrole-to-OH ratio for the quadratic regressions presented in the top panel. The red lines and the equations correspond to linear regressions adjusted on the experimental results. The experiment performed using dry zero air (Pyrrole-to-OH ratio of 3.9) is not included in the linear regressions (see text).

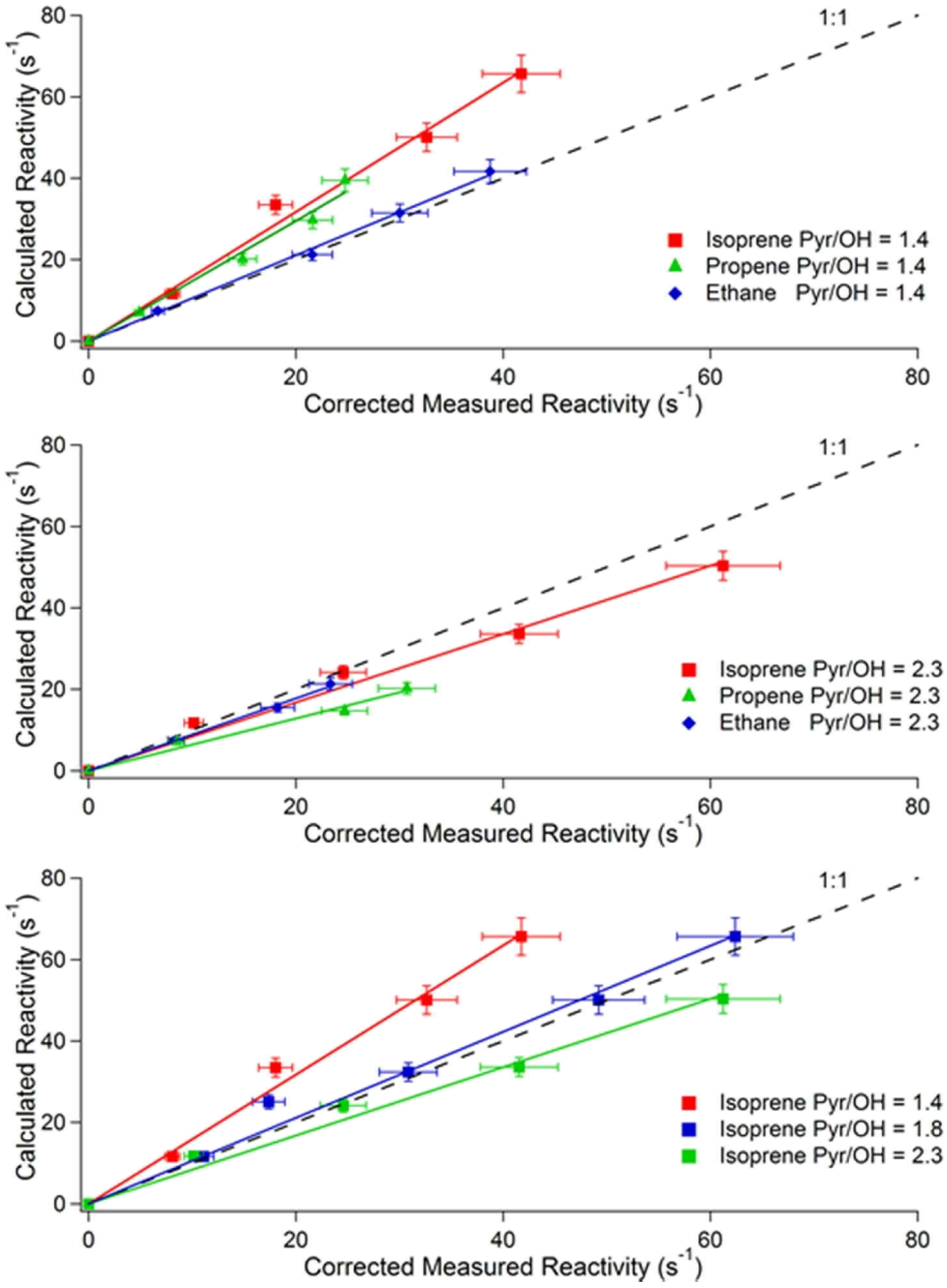


Figure 6: Experimental parameterization of the artifact caused by not operating the instrument under pseudo-first-order conditions. Comparison of OH reactivity values calculated from the addition of gas standards to measured values. Top panel: addition of three different gas standards (Isoprene: red squares, Ethane: blue diamonds, and Propene: green triangles) at a pyrrole-to-OH ratio of 1.4. Middle panel: addition of the three gas standards at a pyrrole-to-OH ratio of 2.3. Bottom panel: addition of isoprene at three different pyrrole-to-OH ratios (1.4: red squares, 1.8: blue squares, and 2.3: green squares).

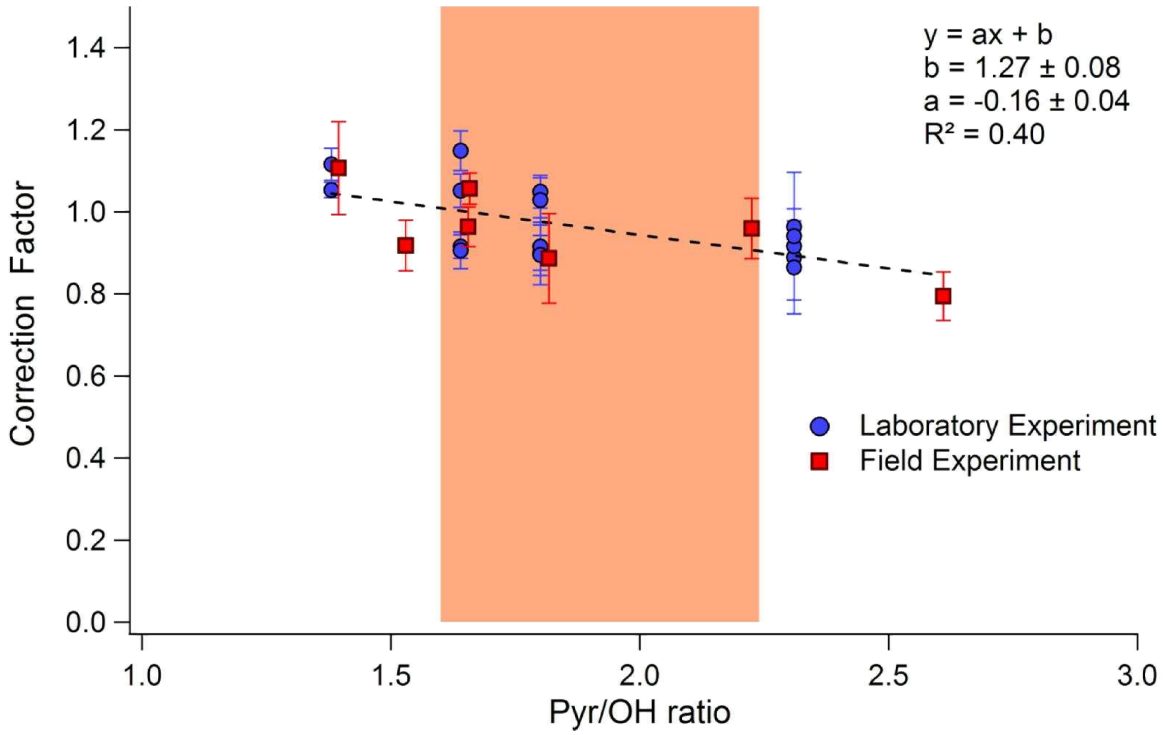


Figure 7 : Dependence of the correction factor *F* on the pyrrole-to-OH ratio. The correction factors were derived from the slopes of scatter plots as shown in Figure 6 for different laboratory (blue circles) and field (red squares) experiments. These experiments were made over a period of 7 months. Error bars are 1σ uncertainties of the slopes determined for each experiment. The colored area is the range of Pyrrole-to-OH ratios observed in the field (1.6-2.2) for the MD-CRM instrument.

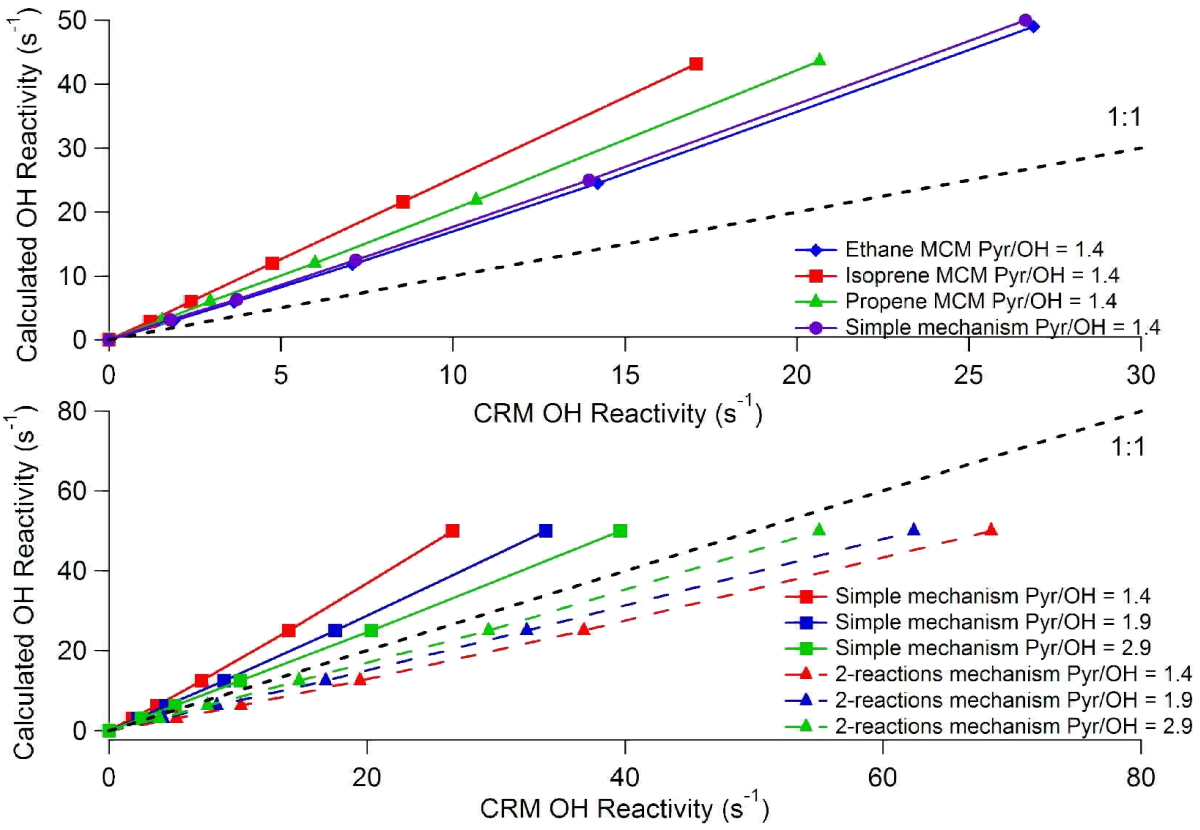


Figure 8 : Simulations of the artifact due to not operating the instrument under pseudo-first-order conditions. Comparison of OH reactivity values calculated from the addition of gas standards to simulated values (simulation of the C1-C2-C3 modulations, see text). Top panel: addition of four different gas standards (Isoprene: red squares, Ethane: blue diamonds, Propene: green triangles, and a surrogate standard for the simple mechanism: purple circles) at a pyrrole-to-OH ratio of 1.4. Simulations were conducted using the MCM and the simple mechanism as indicated in the legend. Bottom panel: addition of a unique standard at three different pyrrole-to-OH ratios (1.4: red symbols, 1.9: blue symbols, and 2.9: green symbols) for simulations conducted with the simple mechanism (squares) and the 2-reaction mechanism (triangles). The gas standard added in the model for these two mechanisms has a reaction rate constant toward OH of 5.0 $10^{-12}$ $cm^3$ $molecules^{-1}$ $s^{-1}$.

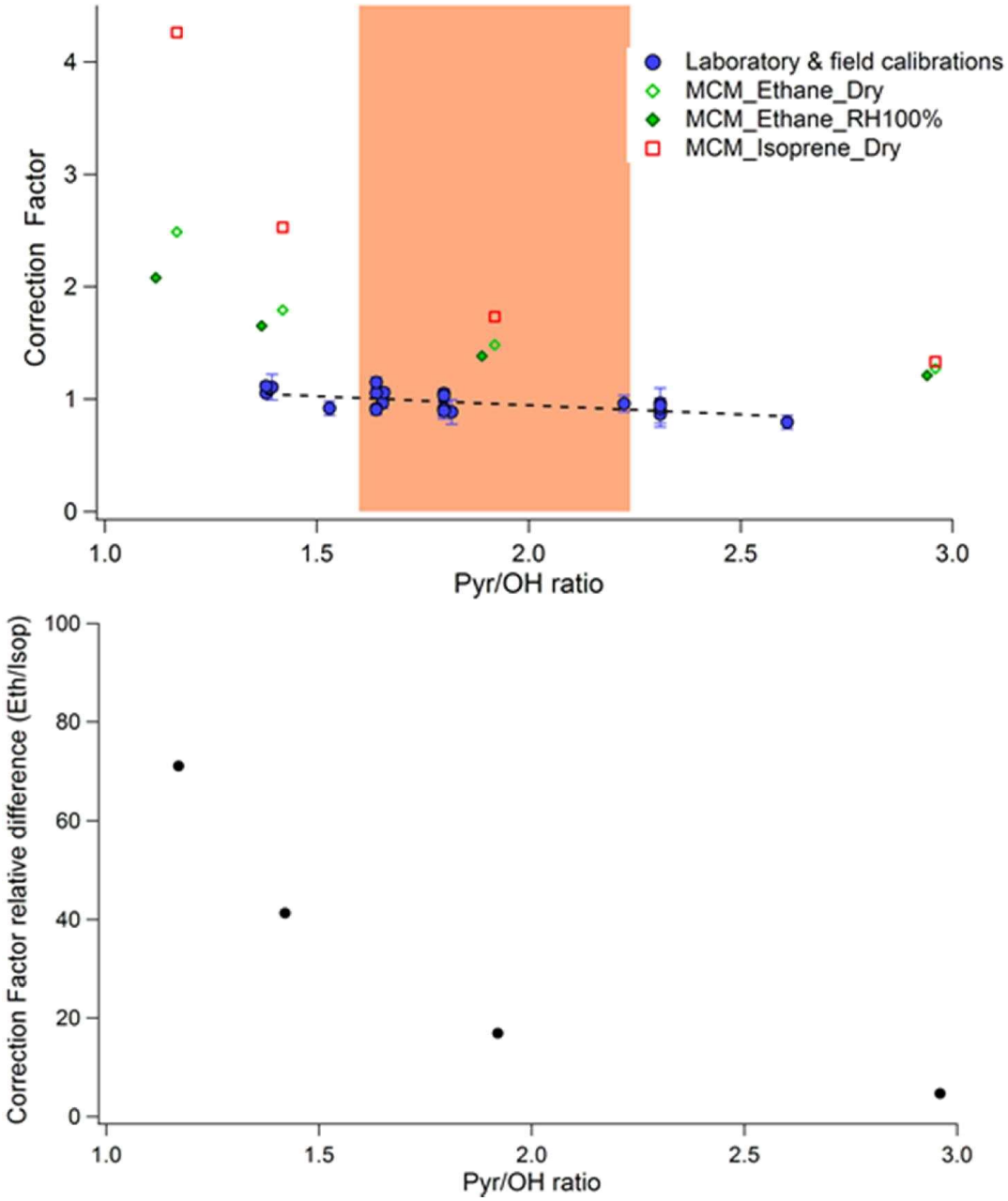


Figure 9: Comparison of model simulations to laboratory observations for the artifact caused by not operating the instrument under pseudo-first-order conditions. Top panel: Trends of the simulated and measured correction factors with the pyrrole-to-OH ratio. The measured correction factors (blues circles) are the same than in Figure 7. The simulated correction factors stem from simulations conducted using MCM and constrained with ethane under dry conditions (green open diamonds) and wet conditions (green filled diamonds), or constrained with isoprene under dry conditions (red open squares). The colored area corresponds to the range of Pyrrole-to-OH ratios observed during field measurements (1.6-2.2). Bottom panel: Trend of the relative difference between correction factors simulated under dry conditions for ethane and isoprene as a function of the pyrrole-to-OH ratio. Relative difference calculated as $100\times(F_{isoprene}-F_{ethane})/F_{ethane}$.

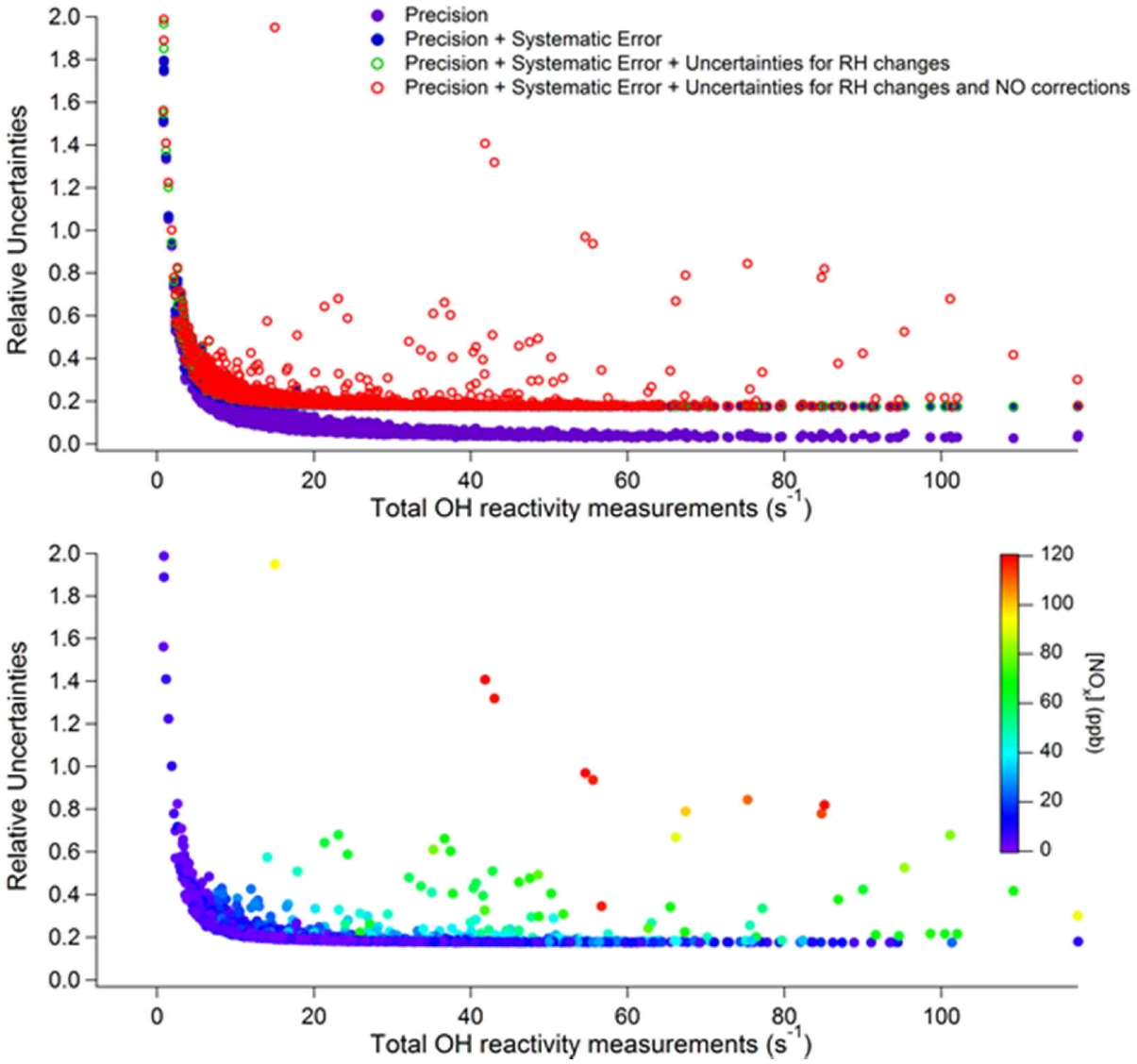


Figure 10: Total OH reactivity measurement uncertainties calculated for the Dunkirk field campaign. Top panel: Precision and relative uncertainty as a function of total OH reactivity. Different levels of uncertainty are considered: (1) the precision observed when measuring the pyrrole signal (purple dots), (2) previous + systematic errors (see text), except for the humidity and NO corrections (blue dots), (3) previous + the humidity correction (green open dots), (4) previous + the NO correction (red open dots). Bottom Panel: Total uncertainty calculated in (4) as a function of total OH reactivity. These data have been color-coded as a function of $NO_x$ levels.

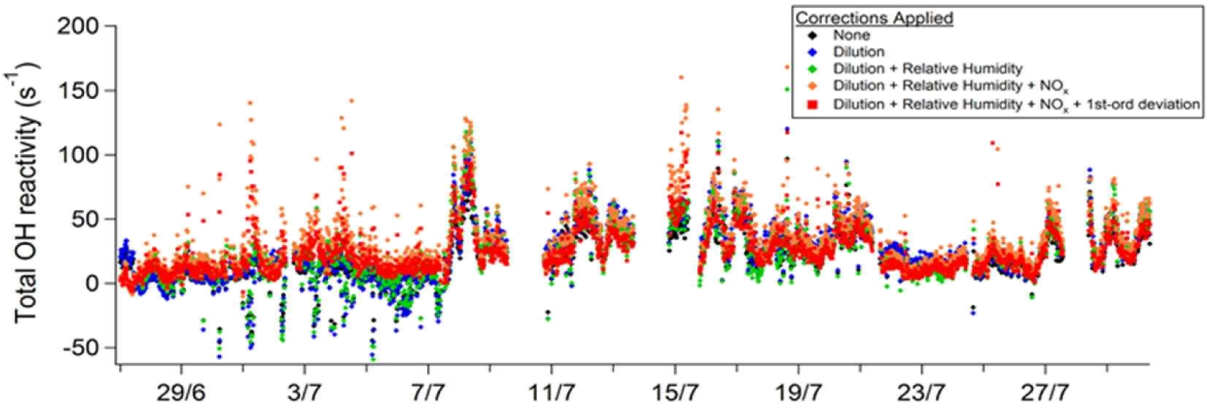


Figure 11: Time series of ambient OH reactivity measurements for the Dunkirk field campaign, including (1) uncorrected measurements (black symbols), (2) measurements corrected for dilution (blue symbols), (3) previous + measurements corrected for differences in relative humidity between C2 and C3 (green symbols); (4) previous + measurements corrected for the NO and $NO_2$ artifacts (orange symbols); (5) previous + measurements corrected for not operating the instrument under pseudo first-order conditions (red symbols). These data are preliminary.